



Contents lists available at ScienceDirect

# Chaos, Solitons and Fractals

Nonlinear Science, and Nonequilibrium and Complex Phenomena

journal homepage: [www.elsevier.com/locate/chaos](http://www.elsevier.com/locate/chaos)

## Recurrence and symmetry of time series: Application to transition detection



Jean-Marc Girault\*

UMR INSERM "Brain &amp; Imaging", U930 University François Rabelais of Tours, France

## ARTICLE INFO

## Article history:

Received 28 October 2014

Accepted 12 April 2015

## ABSTRACT

The study of transitions in low dimensional, nonlinear dynamical systems is a complex problem for which there is not yet a simple, global numerical method able to detect chaos–chaos, chaos–periodic bifurcations and symmetry-breaking, symmetry-increasing bifurcations. We present here for the first time a general framework focusing on the symmetry concept of time series that at the same time reveals new kinds of recurrence. We propose several numerical tools based on the symmetry concept allowing both the qualification and quantification of different kinds of possible symmetry. By using several examples based on periodic symmetrical time series and on logistic and cubic maps, we show that it is possible with simple numerical tools to detect a large number of bifurcations of chaos–chaos, chaos–periodic, broken symmetry and increased symmetry types.

© 2015 Elsevier Ltd. All rights reserved.

### 1. Introduction

For over a century, many researchers have studied the dynamic changes in nonlinear dynamical systems because understanding transitions between regular, laminar and chaotic behaviors is essential to understand the underlying mechanisms behind complex systems. Most studies were performed on the only available practical information, i.e. time series. In view of its ubiquity, studying time series is today an essential and challenging step to forecasting and detecting transitions. This is particularly the case, for instance, in meteorology [1,2] in order to predict the weather effectively, and in medicine to detect the precise instant in time when a stroke occurs, when the patient goes from a normal to an abnormal state [3,4].

From a physical point of view, these changes in operating regime can occur during different kinds of transitions such as periodic–chaos [5], chaos–chaos [4], and hyperchaos–chaos [6] and also during symmetry-breaking bifurcations, [7], to name but a few. Most studies that have investigated these

dynamic changes have analyzed the links between neighboring points in the reconstructed phase space.<sup>1</sup> Studying links between neighboring points in the phase space [8–10] and studying patterns in time series [11] have provided two very popular concepts, i.e. recurrence and symmetry, that have been studied independently until now.

The recurrence concept<sup>2</sup> is an intrinsic and essential property of nonlinear dynamical systems capable of becoming chaotic. Poincaré was the first who formulated a theory and was able to prove the existence of recurrence in dynamical systems mathematically. This recurrence concept, that is based on the presence of recurrent patterns, suggests a certain pattern predictability that allows discrimination between deterministic or stochastic time series from chaotic time series [12,13]. It was Eckmann et al. [8], who a century after Poincaré proposed for the first time a simple numerical

\* Tel.: +33 247361081; fax: +33 247366120.  
E-mail address: [jean-marc.girault@univ-tours.fr](mailto:jean-marc.girault@univ-tours.fr)

<sup>1</sup> This phase space is reconstructed from the only information available concerning the time series. By seeking the correct delays and the embedded dimension, this reconstructed phase space has the same topological properties as the unknown real phase space.

<sup>2</sup> The recurrence theorem states that from a certain time the trajectories of the system repeatedly go as close as possible to the initial trajectory.

tool capable of projecting the recurrence information of a  $d$ -dimensional system into a bidimensional space. Due to its ease of implementation, the analysis of recurrence plots of nonlinear dynamical systems has increased markedly, as reported by Webber et al. [14], and has spread into almost all scientific fields [12,14–19]. From a practical point of view, before evaluating a recurrence plot, it is necessary to reconstruct a phase space trajectory equivalent to the original and inaccessible phase space by embedding the one-dimensional time series into a  $d$ -dimensional space. To do this, a procedure that consists of determining the appropriate delays and embedding dimension must be performed [20].

The symmetry concept is in turn a concept that is much more general than the recurrence concept since it applies to all physical laws encountered in nature. Although many books and articles have been published on the symmetry concept, we propose here a small selection [21–25]. This very common theoretical concept that shows the spatio-temporal invariance properties of systems has been much studied through the phase space representation to observe symmetry breaking [27]. This is particularly the case for nonlinear dynamical systems such as systems having on-off intermittency [28], those with a strongly damped pendulum system [29] and the Helmholtz–Duffing oscillator [7]. There are a certain number of analytical tools to study symmetry bifurcations [30–32]. However, there are no simple numerical tools as for recurrence plots that make it possible to qualify the symmetry changes on the basis of knowledge of only the time series. A simple numerical solution is thus required to quantify the gain or the partial loss of symmetry [33].

In this paper, we present for the first time a general framework that gathers together the concepts of recurrence and symmetry, and at the same time reveals new kinds of recurrence. The study was approached through symmetry recurrence analysis. On the basis of this general framework, a set of simple numerical tools is presented to qualify and then to quantify the presence of symmetric recurrences in the phase space or symmetric patterns in time series. To familiarize the reader with this new kind of tool, periodic time series are presented first. Finally, examples of different types of transition of low dimension nonlinear systems such as logistic and cubic maps are tested and validated through time series.

## 2. Recurrence and symmetry of time series

In order to present the new numerical tools allowing the qualification and quantification of symmetries in a time series, it seemed appropriate to introduce the recurrence concept as a starting point of the symmetry concept. To do so, the commonly used test leading to the calculation of the recurrence matrix is presented first. This test was reformulated in such a way as to introduce the symmetry concept through geometrical transformations known as isometries and adapted for the study of time series. Finally, symmetry matrices complemented by symmetrical descriptors were used to quantify the presence of symmetries in time series.

### 2.1. Recurrence

The recurrence plot concept initially proposed by Eckmann et al. [8] was developed to establish the presence of

similar neighboring points of time series  $x(n)$  derived from an embedding process that consisted first of finding a time delay  $\tau$  and embedded dimension  $d$  and then of reconstructing a phase space topologically similar to the original one. From a  $d$ -dimensional phase space, two points  $\mathbf{X}(m)$  and  $\mathbf{X}(n)$  are considered recurrent if the following test is proved [8]:

$$\|\mathbf{X}(m) - \mathbf{X}(n)\| \leq \epsilon \quad (1)$$

where  $\epsilon$  is a threshold set at 0.1 times the standard deviation of the time series and  $\|\cdot\|$  a norm, and where  $\mathbf{X}(m) = \{x_1(m), x_2(m), \dots, x_d(m)\}$  and  $\mathbf{X}(n) = \{x_1(n), x_2(n), \dots, x_d(n)\}$  are vectors composed of subsignals  $x_i(n)$  believed to be independent and normalized. Subsignals  $x_l$  composed of  $N$  points are functions  $f_l[x]$  of the single available time series  $x(n)$  with  $l = \{1, \dots, d\}$ . Usually, such subsignals  $x_l(n)$  are delayed versions of  $x(n)$  such as:

$$x_l(n) = f_l[x(n)] = x(n - (l - 1)\tau), \quad (2)$$

the delay  $\tau$  being chosen to minimize an independent condition between subsignals  $x_l(n)$ . Note that such a function  $f_l[x(n)]$  can also be based on a derivative for which no delay  $\tau$  has to be found [36].

From Eq. (1), the NxN recurrence matrix  $\mathbf{M}$  can be evaluated. From the phase space, the elements of  $\mathbf{M}$  are defined as:

$$\mathbf{M}(m, n) = \Theta[\epsilon - \|\mathbf{X}(m) - \mathbf{X}(n)\|], \quad (3)$$

where  $\Theta[\cdot]$  is the Heaviside function and  $\|\cdot\|$  is a norm. Nonzero elements of  $\mathbf{M}$  represent similar states while zero elements represent rather different states.

Depending on the value  $d$ , sometimes the recurrence matrix  $\mathbf{M}$  can be contaminated by false recurrences [34,35]. As suggested by [36], it is possible to reduce the presence of such sojourn points drastically by taking  $d \geq 2$ . In the following  $d$  is set at  $d = 2$ .

### 2.2. Isometry and symmetry

To show that the concept of recurrence is a much more general concept than the current concept, it is only necessary to show that there is a test encompassing the test reported in Eq. (1). In this case, the more general test is written as follows:

$$\|\mathbf{X}(m) - \mathbf{G}[\mathbf{X}(k)]\| \leq \epsilon \quad (4)$$

and the corresponding elements of the new matrix  $\mathbf{M}$  can be defined in a general framework as:

$$\mathbf{M}(m, k) = \Theta[\epsilon - \|\mathbf{X}(m) - \mathbf{G}[\mathbf{X}(k)]\|]. \quad (5)$$

where  $\mathbf{G}[\mathbf{X}(k)] = \mathbf{X}'(n)$  is a function that can be directly related to isometry transformation. An isometry is a linear and homogeneous transformation [39] that preserves length. As the object to be studied was a time series of discrete nature, it seemed logical to limit this study to point-transformations, i.e. operating locally at each point.

In the bidimensional space, isometries are affine transformations defined as follows:

$$\mathbf{G}[\mathbf{X}(k)] = \mathbf{X}'(n) = \mathbf{A}\mathbf{X}(k) + \mathbf{B} \quad (6)$$

where  $\mathbf{X}'(n) = \begin{pmatrix} x'_1(n) \\ x'_2(n) \end{pmatrix}$ ,  $\mathbf{A} = \begin{pmatrix} a & b \\ c & d \end{pmatrix}$ ,  $\mathbf{X}(k) = \begin{pmatrix} x_1(k) \\ x_2(k) \end{pmatrix}$ ,  $\mathbf{B} = \begin{pmatrix} e \\ f \end{pmatrix}$ .

**Table 1**

Matrices involved in the  $\mathbf{G}_{p,q}$  isometry operating in the phase space.  $\mathbf{B}_{p,q}$  and  $\mathbf{A}_{p,q}$  where  $p$  and  $q$  are natural numbers  $\in (0, 1)$ . Note that  $\mathbf{A}_{0,0} = -\mathbf{A}_{1,0}$  and  $\mathbf{A}_{0,1} = -\mathbf{A}_{1,1}$ . First kind isometries are obtained for  $q = 0$  and second kind isometries are obtained for  $q = 1$ . Identity and opposite recurrences are obtained for the first kind of isometry. Even and odd recurrences are obtained for the second kind of isometry.

Isometry in phase space	Kinds of recurrence	$p$	$q$	$\mathbf{B}_{p,q}$	$\mathbf{A}_{p,q}$
Identity	1st kind, simple	0	0	$(\begin{smallmatrix} 0 & 0 \\ 0 & 0 \end{smallmatrix})$	$(\begin{smallmatrix} 1 & 0 \\ 0 & 1 \end{smallmatrix})$
Inversion	1st kind, opposite	1	0	$(\begin{smallmatrix} 2\bar{x}_1 \\ 2\bar{x}_2 \end{smallmatrix})$	$(\begin{smallmatrix} -1 & 0 \\ 0 & -1 \end{smallmatrix})$
Horizontal reflection	2nd kind, horizontal	1	1	$(\begin{smallmatrix} 2\bar{x}_1 \\ 0 \end{smallmatrix})$	$(\begin{smallmatrix} -1 & 0 \\ 0 & 1 \end{smallmatrix})$
Vertical reflection	2nd kind, vertical	0	1	$(\begin{smallmatrix} 0 \\ 2\bar{x}_2 \end{smallmatrix})$	$(\begin{smallmatrix} 1 & 0 \\ 0 & -1 \end{smallmatrix})$

**Table 2**

Matrices involved in  $\mathbf{H}_{p,q}$  isometry operating in the time domain.  $\mathbf{D}_{p,q}$  and  $\mathbf{C}_{p,q}$  for different discrete values of  $p$  and  $q \in (0, 1)$ . Note that  $\mathbf{C}_{0,0} = -\mathbf{C}_{1,0}$  and  $\mathbf{C}_{0,1} = -\mathbf{C}_{1,1}$ .

Isometry (time domain)	$p$	$q$	$\mathbf{D}_{p,q}$	$\mathbf{C}_{p,q}$
Translation	0	0	$(\begin{smallmatrix} h_{0,0} \\ 0 \end{smallmatrix})$	$(\begin{smallmatrix} 1 & 0 \\ 0 & 1 \end{smallmatrix})$
Vertical reflection	0	1	$(\begin{smallmatrix} h_{0,1} \\ 0 \end{smallmatrix})$	$(\begin{smallmatrix} -1 & 0 \\ 0 & 1 \end{smallmatrix})$
Inversion	1	0	$(\begin{smallmatrix} h_{1,0} \\ 0 \end{smallmatrix})$	$(\begin{smallmatrix} -1 & 0 \\ 0 & -1 \end{smallmatrix})$
Glide reflection	1	1	$(\begin{smallmatrix} h_{1,1} \\ 0 \end{smallmatrix})$	$(\begin{smallmatrix} 1 & 0 \\ 0 & -1 \end{smallmatrix})$

Isometry conditions prove  $x_1'^2(n) + x_2'^2(n) = x_1^2(k) + x_2^2(k)$  involving  $a^2 + c^2 = 1$ ,  $b^2 + d^2 = 1$  and  $ab + cd = 0$  [39]. When the determinant of  $\mathbf{A}$  is equal to one, isometries are of first kind or of displacement/translation. When it is equal to minus one, isometries are of second kind or of reversal.

In the phase space, four kinds of isometry are necessary to describe the four kinds of symmetry present in a time series. In the phase space the first kind isometries are identity/translation and inversion (see Table 1 when  $q = 0$ ), and the second kind isometries are vertical reflection and horizontal reflection (see Table 1 when  $q = 1$ ). In this case, Eq. (6) can be reformulated as follows:

$$\mathbf{G}_{pq}[\mathbf{X}(k)] = \mathbf{X}'(n) = \mathbf{A}_{pq}\mathbf{X}(k) + \mathbf{B}_{pq}. \quad (7)$$

$p$  and  $q$  are natural numbers  $\in (0, 1)$  and  $\mathbf{A}_{pq} = (\begin{smallmatrix} (-1)^p & 0 \\ 0 & (-1)^{p+q} \end{smallmatrix})$  and  $\mathbf{B}_{pq} = (\begin{smallmatrix} 1-(-1)^p\bar{x}_1 \\ 1-(-1)^{p+q}\bar{x}_2 \end{smallmatrix})$  with  $\bar{x}_i = (x_i(k) + x'_i(n))/2$ .

Similarly to Eq. (4), another test can be proposed:

$$\|\mathbf{X}(m) - \mathbf{G}_{pq}[\mathbf{X}(k)]\| \leq \epsilon, \quad (8)$$

and the corresponding elements of the matrix  $\mathbf{M}_{pq}$  can be defined as:

$$\mathbf{M}_{pq}(m, k) = \Theta[\epsilon - \|\mathbf{X}(m) - \mathbf{G}_{pq}[\mathbf{X}(k)]\|]. \quad (9)$$

Note that there is another possible way to describe symmetry in a time series. As for current recurrence analysis, it is possible to extract symmetry without embedding, i.e. directly from a single time series. In the time domain, four kinds of isometry are necessary to describe the four kinds of symmetry present in a time series. In the time domain these isometries are: translation, vertical reflection, inversion and glide reflection (see Table 2). In this case, Eq. (7) can be refor-

mulated as follows:

$$\mathbf{Y}(n) = \mathbf{H}_{pq}[\mathbf{Y}(k)] = \mathbf{C}_{pq}\mathbf{Y}(k) + \mathbf{D}_{pq}, \quad (10)$$

where  $p$  and  $q \in (0, 1)$  are natural numbers, with  $\mathbf{Y}(n) = (\begin{smallmatrix} n \\ x'_i(n) \end{smallmatrix})$ ,  $\mathbf{Y}(k) = (\begin{smallmatrix} k \\ x_i(k) \end{smallmatrix})$ ,  $\mathbf{C}_{pq} = (\begin{smallmatrix} (-1)^{p+q} & 0 \\ 0 & (-1)^p \end{smallmatrix})$  and  $\mathbf{D}_{pq} = (\begin{smallmatrix} h_{p,q} \\ 0 \end{smallmatrix})$ ,  $h_{p,q}$  being a delay that depends on the time series under study.

Similarly to Eq. (4), another test can be proposed:

$$\|\mathbf{Y}(m) - \mathbf{H}_{pq}[\mathbf{Y}(k)]\| \leq \epsilon, \quad (11)$$

and the corresponding elements of the matrix  $\mathbf{M}'_{pq}$  can be defined as:

$$\mathbf{M}'_{pq}(m, k) = \Theta(\epsilon - \|\mathbf{Y}(m) - \mathbf{H}_{pq}[\mathbf{Y}(k)]\|). \quad (12)$$

As an illustration (see Fig. 1), we can determine analytically the four matrices  $M_{00}, M_{01}, M_{10}, M_{11}$  and the symmetry elements such as time delays, inversion centers or reflection axes, that are representative of a symmetrical time series  $x(n)$  proving the global odd symmetry property  $x(n) = -x(-n)$ . A periodic triangular time series  $x(n)$  or its harmonic components (of period  $\beta T_0 \forall \beta \in \mathcal{Z}$ ) can be considered arbitrary as they share the same symmetry properties. Solution of the problem comes down to calculating the temporal parameter  $h_{pq}^*$  verifying the following equation:

$$h_{pq}^* = \arg \min_h (\|\mathbf{X}(k+h) - (\mathbf{A}_{pq}\mathbf{X}(k) + \mathbf{B}_{pq})\|) \quad (13)$$

To solve the problem with the embedding procedure, we considered two subsignals  $x_1(n) = x(n)$  and  $x_2(n) = x_1(n - T_0/4)$  derived from  $x(n)$ . For a periodic time series, the harmonic components can be considered as follows  $x_1(n) = \sin(\beta\omega_0 n)$  and  $x_2(n) = \cos(\beta\omega_0 n)$  with  $\beta \in \mathcal{Z}^*$ . As reported for the phase space (see Fig. 1a with  $\beta = 1$ ), the attractor of the triangular time series is a square, with a circle for each harmonic component. The four isometries reported in Fig. 1 can be considered for this kind of time series. The first two are of the first kind and the last two are of the second kind.

- For the “Identity/translation” isometry obtained for  $p = 0$  and  $q = 0$  (reported in Fig. 1a), the parameter  $h_{00}^*$  minimizing Eq. 13 can be obtained from the following system:

$$\begin{cases} \sin(\beta\omega_0(k + h_{00}^*)) - \sin(\beta\omega_0 k) = 0, \\ \cos(\beta\omega_0(k + h_{00}^*)) - \cos(\beta\omega_0 k) = 0. \end{cases} \quad (14)$$

The resolution of the previous equation system leads to  $h_{00}^* = \alpha\beta T_0$  with  $\alpha \in \mathcal{Z}$  and  $\beta \in \mathcal{Z}^*$  for all harmonic

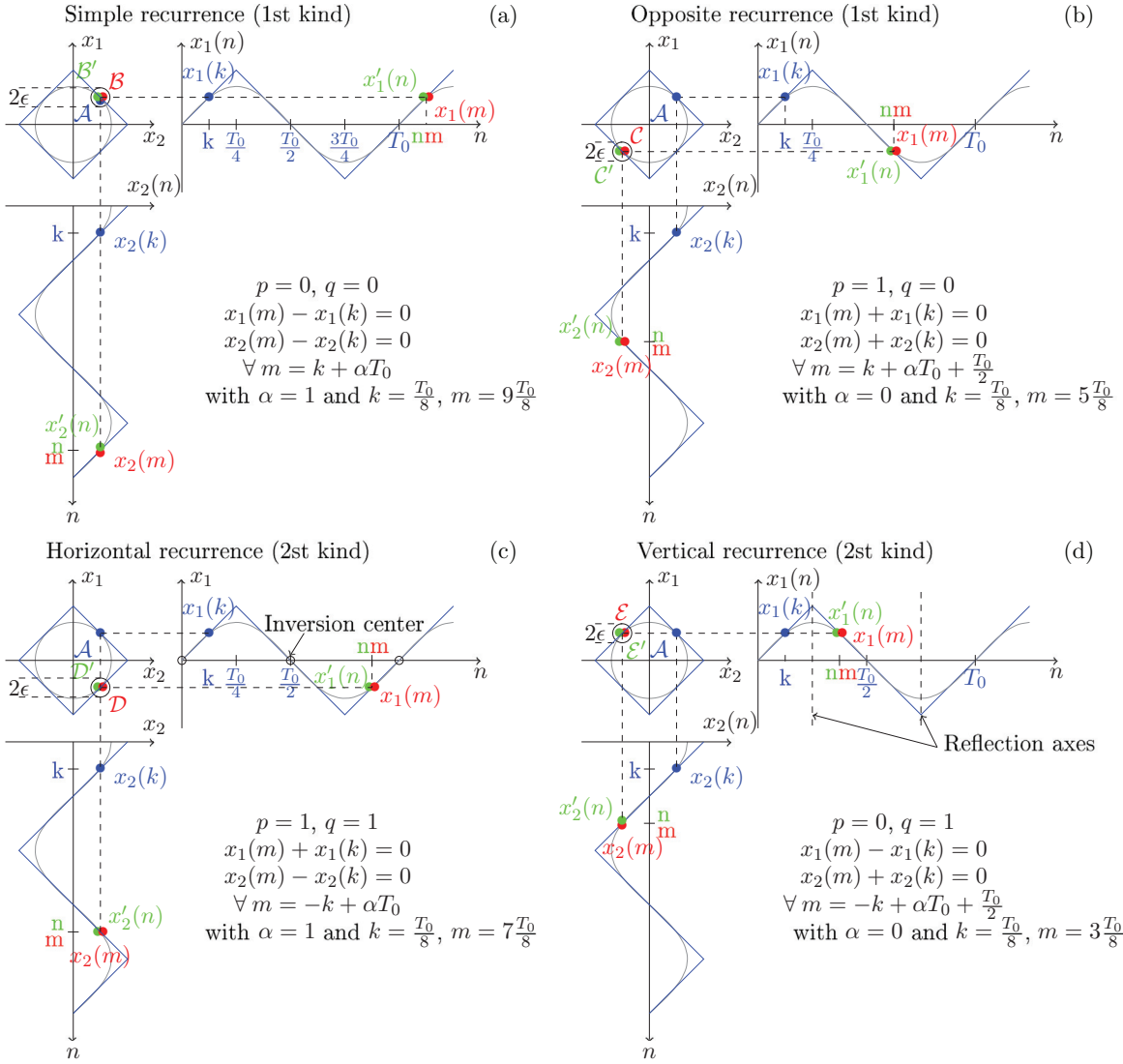


**Fig. 1.** Temporal representations of a triangular periodic time series and its fundamental component  $\beta = 1$  and their corresponding attractors in the phase space. Triangular subsignal  $x_1(n)$  is represented by a blue line and its fundamental component by a gray line. Triangular orthogonal subsignal  $x_2(n)$  is a blue line and its fundamental component is a gray line. In the phase space, the attractors of the triangular signal and of its fundamental component are represented by a square (blue) and a circle, respectively. (a) Isometry “Identity”. Points  $B'$  (image of  $A$ ) and  $B$  represent recurrence points since they are inside the circle of diameter  $2\varepsilon$ . In the time domain, simple recurrence points are similar points shifted by  $\alpha T_0$ :  $x_i(m) = x_i(k + \alpha T_0)$  with  $i = 1, 2$ . With  $\alpha = 1$  and  $k = T_0/8$ , the symmetrical point is located at  $m = 9T_0/8$ . (b) Isometry “Inversion”. Points  $C'$  (image of  $A$ ) and  $C$  represent opposite points since they are inside the circle of diameter  $2\varepsilon$ . In the time domain, symmetrical points are similar points proving:  $x_1(m) = -x_1(k + \alpha T_0 + T_0/2)$  and  $x_2(m) = -x_2(k + \alpha T_0 + T_0/2)$ . With  $\alpha = 0$  and  $k = T_0/8$ , the symmetrical point is located at  $m = 5T_0/8$ . (c) Isometry “Horizontal Reflection”. Points  $D'$  (image of  $A$ ) and  $D$  represent horizontal mirror points since they are inside the circle of diameter  $2\varepsilon$ . In the time domain, symmetrical points are similar points proving:  $x_1(m) = -x_1(-k + \alpha T_0)$  and  $x_2(m) = x_2(-k + \alpha T_0)$ . With  $\alpha = 1$  and  $k = T_0/8$ , the symmetrical point is located at  $m = 7T_0/8$ . (d) Isometry “Vertical Reflection”. Points  $E'$  (image of  $A$ ) and  $E$  represent vertical mirror points since they are inside the circle of diameter  $2\varepsilon$ . In the time domain, symmetrical points are similar points proving:  $x_1(m) = x_1(-k + \alpha T_0 + T_0/2)$  and  $x_2(m) = -x_2(-k + \alpha T_0 + T_0/2)$ . With  $\alpha = 0$  and  $k = T_0/8$ , the symmetrical point is located at  $m = 3T_0/8$ . (For interpretation of the references to color in this figure legend, the reader is referred to the web version of this article.)

components of the triangular time series. These kinds of recurrence correspond to the first kind of recurrence. Such recurrences, called simple recurrences, correspond to translations within  $x_1(n)$  and  $x_2(n)$ . Matrix  $M_{00}$  is equal to unity when the time delay  $h = h_{00}^*$  and is null otherwise.

- For the “inversion” isometry, obtained for  $p = 1$  and  $q = 0$  (reported in Fig. 1b), the parameter  $h_{10}^*$  minimizing Eq. 13 is obtained from the following system:

$$\begin{cases} \sin(\beta\omega_0(k + h_{10}^*)) + \sin(\beta\omega_0 k) = 0, \\ \cos(\beta\omega_0(k + h_{10}^*)) + \cos(\beta\omega_0 k) = 0. \end{cases} \quad (15)$$

The resolution of the previous equation system leads to  $h_{10}^* = \beta T_0/2 + \alpha\beta T_0$  with  $\alpha \in \mathbb{Z}$  and  $\beta \in \mathbb{Z}^*$  for all harmonic components of the triangular time series. These kinds of recurrence correspond to the first kind of recurrence. Such recurrences, called opposite recurrences,

correspond to glides (translation with opposite values) within  $x_1(n)$  and  $x_2(n)$ . Matrix  $\mathbf{M}_{10}$  is equal to unity when the time delay  $h = h_{10}^*$  and is null otherwise;

- For the “horizontal reflection” isometry, obtained for  $p = 1$  and  $q = 1$  (reported in Fig. 1c), the parameter  $h_{11}^*$  minimizing Eq. 13 is obtained from the following system:

$$\begin{cases} \sin(\beta\omega_0(k + h_{11}^*)) + \sin(\beta\omega_0k) = 0, \\ \cos(\beta\omega_0(k + h_{11}^*)) - \cos(\beta\omega_0k) = 0. \end{cases} \quad (16)$$

The resolution of the previous equation system leads to  $h_{11}^* = -2k + \alpha\beta T_0$  with  $\alpha \in \mathcal{Z}$  and  $\beta \in \mathcal{Z}^*$  for all harmonic components of the triangular time series. Note that each inversion center is separated by  $\beta T_0/2$ , the first position of the inversion center being located at 0. These kinds of recurrence correspond to the second kind of recurrence. Such recurrences, called horizontal recurrences, correspond to translations/odd symmetries within  $x_1(n)$  and  $x_2(n)$ . Matrix  $\mathbf{M}_{11}$  is equal to unity when the time delay  $h = h_{11}^*$  and is null otherwise.

- For the “vertical reflection” isometry, obtained for  $p = 0$  and  $q = 1$  (reported in Fig. 1b), the parameter  $h_{01}^*$  minimizing Eq. 13 is obtained from the following system:

$$\begin{cases} \sin(\beta\omega_0(k + h_{01}^*)) - \sin(\beta\omega_0k) = 0, \\ \cos(\beta\omega_0(k + h_{01}^*)) + \cos(\beta\omega_0k) = 0. \end{cases} \quad (17)$$

The resolution of the previous equation system leads to  $h_{01}^* = -2k + \alpha\beta T_0 + \beta T_0/2$  with  $\alpha \in \mathcal{Z}$  and  $\beta \in \mathcal{Z}^*$  for all harmonic components of the triangular time series. Note that reflection axes are separated by  $\beta T_0/2$ , the first reflection axis being located at  $\beta T_0/4$ . These kinds of recurrence correspond to the second kind of recurrence. Such recurrences, called vertical recurrences, correspond to even/odd symmetries within  $x_1(n)$  and  $x_2(n)$ . Matrix  $\mathbf{M}_{01}$  is equal to unity when the time delay  $h = h_{01}^*$  and is null otherwise;

To sum up this section, four new recurrences with different symmetry properties were demonstrated. As shown in the illustration, the corresponding matrices were sensitive to the presence of different kinds of symmetry. A quantification step is necessary to go further in the symmetry recurrence analysis, as for instance to differentiate local and global symmetries.

### 2.3. Descriptors : symmetry quantification analysis

As shown in the previous section, the recurrence notion can be extended to the concept of symmetric recurrence. To quantify these new kinds of recurrence, it seems advisable to extend the existing recurrence descriptors to the new types of recurrence. Consequently, based on recurrence quantification analysis (RQA) previously introduced in the early 1990s [20], “symmetry quantification analysis” (SQA) can be introduced to quantify changes in operating regime without making any a priori assumptions regarding the unknown underlying equations. As systems to be studied may be stable or unstable, and may generate periodic or chaotic time series, antinomic descriptors sensitive to periodic or chaotic behavior were proposed. To describe periodic properties, the percentage of points making up the anti-diagonal/diagonal

segments ( $DET_{p,q}$ ) were proposed. In contrast to periodic properties, chaotic descriptors defined as the inverse length of the longest diagonal segment  $DIV_{p,q}$  were proposed. Note that, though a large number of symmetry descriptors (SD) based on RQA [4,20] might be proposed, a limited number of SD were tested here to validate the concept simply.

- The simplest group of recurrence descriptors is the one that counts the percentage of symmetric recurrence points present in the matrix  $M_{p,q}$ . The first group of symmetrical descriptors  $DP_{p,q}$  quantifies the number of pairs of recurring 2-tuples that are symmetric.  $DP_{p,q}$  is the probability that a state recurs in its  $\varepsilon$ -neighborhood in phase space, whatever the type of symmetry. These descriptors are written:

$$DP_{p,q} = \frac{1}{N^2} \sum_{n,k=1}^N M_{p,q}(n, k) \quad \forall n \neq k \quad (18)$$

with natural numbers  $p, q \in \{0, 1\}$ . These descriptors, that may vary between 0 and 1, are a kind of correlation sum initially defined by [37] and are sensitive to each kind of symmetry by simply counting the presence of similar states, i.e. the coincidence of pairs of d-tuples in d subsignals ( $d = 2$  in this study). The points belonging to the main diagonal are not taken into account and self-recurrences are discarded;

- In contrast to  $DP$ , the next group of descriptors describes links that last over time, the presence of temporal correlations being related to the notion of predictability and determinism. As the temporal links appear through the presence of diagonals/anti-diagonals, the second group of symmetrical descriptors ( $DET_{p,q}$ ) quantifies the percentage of points that formed diagonal or anti-diagonal segments in relation to the total number of recurrence points. Indeed, the lengths of diagonals represent the average time that two points of the trajectory are close to each other and can be interpreted as the mean prediction time. In the case of periodic time series, this duration is the period of the time series. These descriptors are written:

$$DET_{p,q} = \frac{\sum_{l=L_{min}}^N l_{p,q} P(l_{p,q})}{N^2 DP_{p,q}} \quad (19)$$

where  $P(l_{p,q})$  is the probability of finding a diagonal/anti-diagonal segment of length  $l_{p,q}$  and  $L_{min}$  the shortest segment length.  $L_{min}$  is often set at 2. The points belonging to the main diagonal are not taken into account. The presence of diagonal/anti-diagonal segments reveals the presence of temporal symmetrical patterns. The presence of several diagonal segments separated by a certain duration can reveal the periodic nature of time series, while very small sparse segments reveal the presence of random time series. Note that when there is no diagonal, the descriptor is not defined and  $DET$  is empty. No value is then plotted;

- Among all possible values of the diagonal lengths,  $L_{max}$  is certainly the most appropriate to quantify the degree of predictability.  $L_{max}$  is an approximation of the characteristic time of the system, sometimes called “Lyapunov horizon”. The inverse of  $L_{max}$  expresses the level of difficulty for forecasting the temporal evolution of systems. The predictability of the system evolution is possible only

for times lower than this horizon. The divergence descriptor  $DIV$  that is the inverse of  $L_{max}$  is an approximation of the largest positive Lyapunov exponent (LLE) characterizing the rate of separation of close trajectories [8]. If the recurrence points belonging to trajectories have symmetric properties, then the divergence indicator is only the image of the divergence rate when symmetry properties are present. In all cases, the faster the trajectory segments diverge, the shorter the diagonal lines and the more chaotic the time series. The last group of descriptors presented here is written:

$$DIV_{p,q} = \frac{1}{L_{\max p,q}} \quad (20)$$

with  $L_{\max p,q} = \max(\{l_{p,q}(k)\}_{k=1}^{N_l})$  that is an approximation of the Lyapunov time horizon and  $N_l = \sum_{l_{p,q} \geq l_{min}} P(l_{p,q})$ . The points belonging to the main diagonal have not been taken into account. Note that when it is not possible to measure the maximum length of diagonals due to the absence of diagonals, the descriptor is not defined and  $DIV$  is empty, no values are plotted.

Given the numerical tools allowing the qualitative and quantitative description of symmetry present in a time series, it seemed essential to test these new tools on simple deterministic time series (see Section 3) and on well-known time series derived from logistic and cubic maps (see Section 4).

### 3. Characterization of deterministic time series

The aim of the work reported in this section was to explore the specific features of deterministic time series possessing different types of symmetry and different levels of symmetry, using analysis of different kinds of recurrence. To analyze the qualitative and quantitative potentials of symmetry plots (SP) and symmetry descriptors (SD), periodic time series with an adjustable duty cycle  $\delta$  were examined. The duty cycle, that changes the symmetry of the time series, plays the role of a symmetry control parameter. When the duty cycle is different from 0.5, the resulting time series is dissymmetric, i.e. with a lack of symmetry. For this purpose, the emphasis was on evaluating invariances on identity/translation, vertical reflection, inversion and horizontal/glide reflection.

A good candidate to analyze global and local symmetry is the triangular periodic time series  $x(n)$  of period  $T_0$ . Two subsignals  $x_1(n)$  and  $x_2(n)$  composed of  $N$  points were derived from  $x(n)$ . The time series  $x_1(n)$ , that is a copy of the original time series  $x(n)$ , is represented for a duration of  $T = 3$  s, i.e. during three periods  $T_0 = 1$  s (see Fig. 2a). This time series is of odd global symmetry since  $x_1(n) = -x_1(-n)$ , the global inversion center being located at  $n = 0$ . Note that, as seen before, due to the periodic nature of such time series, there are an infinite number of inversion centers located at  $\alpha T_0/2$ ,  $\forall \alpha \in \mathbb{Z}$ .  $x_2(n)$  is a time series orthogonal to  $x_1(n)$ .  $x_2(n)$  can be a delayed version of  $x_1(n)$  with  $\tau = T_0/4$  or the derivative of  $x(n)$ . The time series  $x_2(n)$  is of even global symmetry since  $x_2(n) = x_2(-n)$ . Note that, as seen before, due to the periodic nature of such time series, there are an infinite number of reflection axes located at  $\alpha T_0/2$ ,  $\forall \alpha \in \mathbb{Z}$ , the first being located at  $n = 0$ .

### 3.1. Qualitative analysis

Symmetry matrices  $M_{0,0}$ ,  $M_{0,1}$ ,  $M_{1,0}$ ,  $M_{1,1}$  derived from the two time series  $x_1(n)$  and  $x_2(n)$  (with embedding) are obtained with  $\varepsilon = 10\%$  times the standard deviation of the time series (set out in Fig. 2). At the top of Fig. 2, the time series  $x_1(n) = x(n)$  with a duty cycle of 50% is represented by a solid blue line and the orthogonal time series  $x_2(n)$  is represented by a red line.

Matrix  $M_{0,0}$  of simple recurrences resulting from the application of the identity isometry matrix (represented in Fig. 2b) shows lines parallel to the main diagonal. These diagonal lines express a global invariance by identity isometry at each period  $T_0$  or by a translation of  $T_0$  into the time series  $x_1(n)$  and  $x_2(n)$ . Because the translation invariance corresponds to the period  $T_0$  of the time series, the diagonals present in the symmetry plot were separated by the period  $T_0$  of 1 s duration. Reading of this matrix indicated that the maximum duration for which consecutive points were invariant was  $T - T_0 = (K - 1)T_0$ , self recurrences not being taken into account. In this figure, the maximum duration of recurrence is  $2T_0 = 2$  s, with  $K = 3$  and  $T = 3$  s.

Matrix  $M_{1,0}$  of opposite recurrences resulting from the application of the inverse isometry matrix (represented in Fig. 2c) shows lines parallel to the main diagonal. These parallel lines express global invariance by inversion isometry at each period  $T_0$  or by translation  $T_0$  of opposite recurrence points (glide) in  $x_1(n)$  and  $x_2(n)$ . Diagonals are separated by the period  $T_0$ . Reading of this matrix indicated that the maximum duration for which consecutive recurring points of opposite amplitude were invariant by glide reflection was about  $(2K - 1)T_0/2$ . In this figure, the maximum duration of opposite recurrence is  $5T_0/2 = 2.5$  s, with  $K = 3$  and  $T = 3$  s.

Symmetry matrix  $M_{1,1}$  of horizontal recurrences resulting from the application of the horizontal reflection isometry matrix (represented in Fig. 2d) shows lines parallel to the second diagonal. These anti-parallel lines express global invariance by horizontal reflection, or by inversion in  $x_1(n)$  and translation in  $x_2(n)$ . For an observation duration of 3 s, there were 6 symmetrical elements that were inversion centers located at  $t = T_0/2, 2T_0/2, 4T_0/2, 6T_0/2, 8T_0/2, 10T_0/2$  (see red circles in Fig. 2d) and separated from each other by  $T_0/2$ . Reading of this matrix indicated that  $N$  points were invariant by inversion (the whole antidiagonal). In other words, the maximum duration for which consecutive points were odd was 100% of the total duration of the time series ( $KT_0 = 3$  s with  $K = 3$ ). Anti-diagonals were separated by the period  $T_0$ .

Symmetry matrix  $M_{0,1}$  of vertical recurrences resulting from the application of the vertical reflection isometry matrix (represented in Fig. 2e) shows lines parallel to the second diagonal. These anti-parallel lines express global invariance by vertical reflection, i.e. even symmetries in  $x_1(n)$  and odd symmetries in  $x_2$  or vice versa. For an observation duration of 3 s, there were 6 symmetrical elements that were reflection axes located at  $t = T_0/4, 3T_0/4, 5T_0/4, 7T_0/4, 9T_0/4, 11T_0/4$  (see red circles in Fig. 2d) and separated from each other by  $T_0/2$ . Reading of this matrix indicated that the maximum duration for which consecutive recurring points were even/odd was about  $(2K - 1)T_0/2$ . In this figure, the maximum duration of recurrence is  $5T_0/2 = 2.5$  s, with  $K = 3$  and  $T = 3$  s. Anti-diagonals in the figure are separated by the period  $T_0$ .

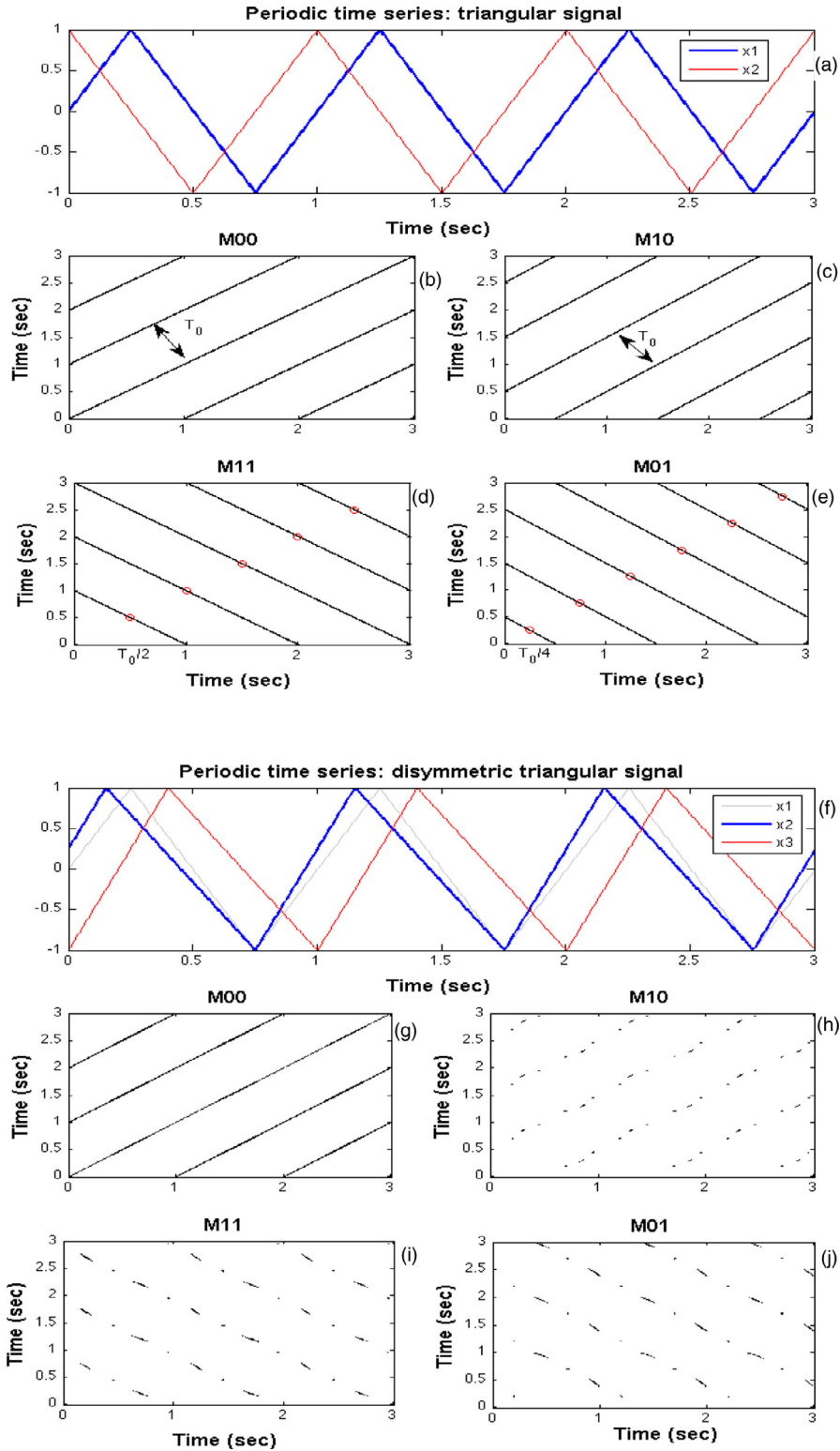


**Fig. 2.** Symmetry plots of symmetric and dissymmetric triangular signals. (a) Triangular time series  $x_1$  and  $x_2$  with a duty cycle  $\delta$  set at 50%. (b) Matrix  $M_{00}$  of simple recurrences. (c) Matrix  $M_{10}$  of opposite recurrence. (d) Matrix  $M_{11}$  of horizontal recurrences. Red circles represent inversion centers. Long diagonals and anti-diagonals show the intrinsic property of global symmetry of the time series examined. Antidiagonals and diagonals are separated by the period  $T_0$ . (e) Matrix  $M_{01}$  of vertical recurrences. Red circles represent reflection axes. (f) Triangular time series  $x_1$  and  $x_2$  with a duty cycle  $\delta$  set at 40%. (g)  $M_{00}$ . (h)  $M_{10}$ . (i)  $M_{11}$ . (j)  $M_{01}$ . Short diagonals and anti-diagonals show local symmetry. (For interpretation of the references to color in this figure legend, the reader is referred to the web version of this article.)

By modifying the duty cycle of the triangular time series, the degree of symmetry changed (see Fig. 2f), a time series of global symmetry being transformed into a time series with local symmetry. The time series represented in Fig. 2f were triangular signals with a 40% duty cycle. As represented in Fig. 2g–j, the lengths of diagonal and anti-diagonal segments were drastically reduced when the duty cycle reduced from 50% to 40%. As diagonals and anti-diagonals did not extend over the entire symmetry plot, the measurements demonstrated that the time series possessed local symmetry. It was demonstrated that variation of the duty cycle led to global or local symmetry.

At that level of the study, the global symmetry of the triangular time series was demonstrated by the presence of diagonals and anti-diagonals that fully occupied the width of the symmetry plots (SP). Although it seems very surprising at first sight, a triangular signal of global odd symmetry also possessed other kinds of global and local symmetry.

### 3.2. Quantitative analysis

In the quantitative analysis, symmetry descriptors (SD) (see Fig. 3a–c) were calculated in relation to the duty cycle. It can be seen from Fig. 3a, that the percentage of points that jointly recurred symmetrically in the two subsignals was less than 5%. This value indicates that over the entire set of possible pairs of points, only 5% recur. Note that all  $DP_{p,q}$  except  $DP_{00}$  increased as the duty cycle increased. These kinds of descriptor seem to be sensitive to the increase in the percentage of symmetrical recurrence points and the degree of symmetry. Maximum symmetry was reached when the duty cycle was maximum ( $\delta = 50\%$ ):  $\max(DP_{01}) = \max(DP_{10}) = \max(DP_{11}) = 2.8\%$ . This shows an obvious link between the presence of recurrence points and the degree of symmetry. The behavior of  $DP_{00}$  was different from the other SD since it decreased as the duty cycle increased, plotting a minimum of recurrence when the duty cycle was maximum ( $\delta = 50\%$ ). We have no hypothesis to explain this kind of behavior, except that it seemed to depend on the kind of time series under study. Note that  $DP$  does not explain temporal correlations whereas  $DET$  substantially explains these temporal links. Indeed, the symmetry descriptors  $DP = 2.8\%$  and  $DET = 99.9\%$  obtained for the triangular time series became  $DP = 2.8\%$  and  $DET = 5.6\%$  after destruction of such links by randomization of temporal indices. It is clear now that the number of symmetrical recurrences is independent of the temporal links between time samples while the number of recurrence points belonging to diagonals is strongly dependent. When the link between samples lasts for the whole time series,  $DET$  approaches 100% and the time series can be qualified as deterministic.

It can be seen from Fig. 3b that most  $DET_{p,q}$  were independent of  $\delta$  and equal to unity, except  $DET_{10}$  that changed suddenly when the duty cycle was in the [5%, 50%] range. In the latter range all  $DET_{p,q}$  were equal to unity, confirming that the time series under analysis was a deterministic time series. These kinds of descriptor seem insensitive to changes in degree of symmetry but suitable to detect the deterministic nature of the time series.

It can be seen from Fig. 3c, that  $DIV_{10}$  decreased toward zero as the duty cycle increased.  $DIV_{10}$  varied from 1/0.0015 =

666.7 with  $L_{max} = 0.0015$  s to 1/2 = 0.5 with  $L_{max} = 2$  s over the whole range, whereas the other parameters varied slightly around 1/3 = 0.33 with  $L_{max} = 3$  s. In all cases,  $DIV_{p,q}$  were close to zero when the duty cycle was maximum, confirming the periodic nature of the time series under study. Indeed, it should be remembered that for such time series the trajectories remain very close, leading to a wide Lyapunov time horizon and a small divergence rate.

To conclude, these first simulations confirmed that there were representations and parameters sensitive to symmetry changes. However, the level of sensitivity was different for each symmetry plot (SP) and symmetry descriptor (SD) and it depended on the kind and the degree of symmetry present in the time series. SP and SD were thus capable of expressing and quantifying global and local symmetries present in a periodic time series. To confirm that SP and SD were still valid to characterize other kinds of time series, chaotic time series were then considered.

## 4. Characterization of chaotic time series

The aim of this section is to present evaluation of the ability of the proposed symmetry plots (SP) and symmetry descriptors (SD) to analyze different kinds of transitions qualitatively and quantitatively, respectively. Periodic-periodic, periodic-chaotic, chaotic-periodic bifurcation points [5] and chaos-chaos transitions [4,38], as well as “symmetry breaking” and “symmetry increasing” [7,27,28] were therefore analyzed by varying the control parameters of different kinds of maps. Two examples were studied: the logistic map and the cubic map. These two systems were interesting since they were simple and, with few modifications of their definitions, they allowed study of both recurrences and symmetries.

### 4.1. The logistic map

In its classical version, the logistic map that does not possess global symmetry is defined by:

$$x_{n+1} = rx_n(1 - x_n), \quad (21)$$

where the control parameter  $r$  is in the range [3.5, 4.0] as suggested in [4,5]. Several distinct dynamic regimes in the transient time series can be easily recognized in this range: period 4, period 8, chaotic, period 6, chaotic, period 5, chaotic, period 3, chaotic, etc. [5].

To highlight the different types of regime changes such as periodic-chaotic, chaotic-periodic and chaotic-chaotic, the largest Lyapunov exponent  $\lambda$  and supertrack functions were evaluated:

- The largest Lyapunov exponent (LLE) defined as follows:

$$\lambda = \frac{1}{N} \sum_{n=1}^N \log_2 |r(1 - 2x_n)|$$

was evaluated in relation to the control parameter  $r$ , as suggested by [5]. For such a system, chaotic regimes were present when the largest Lyapunov exponent was positive  $\lambda > 0$ .

- To confirm the chaotic-chaotic transitions reported by Marwan et al. [4], recursive functions named “supertrack”

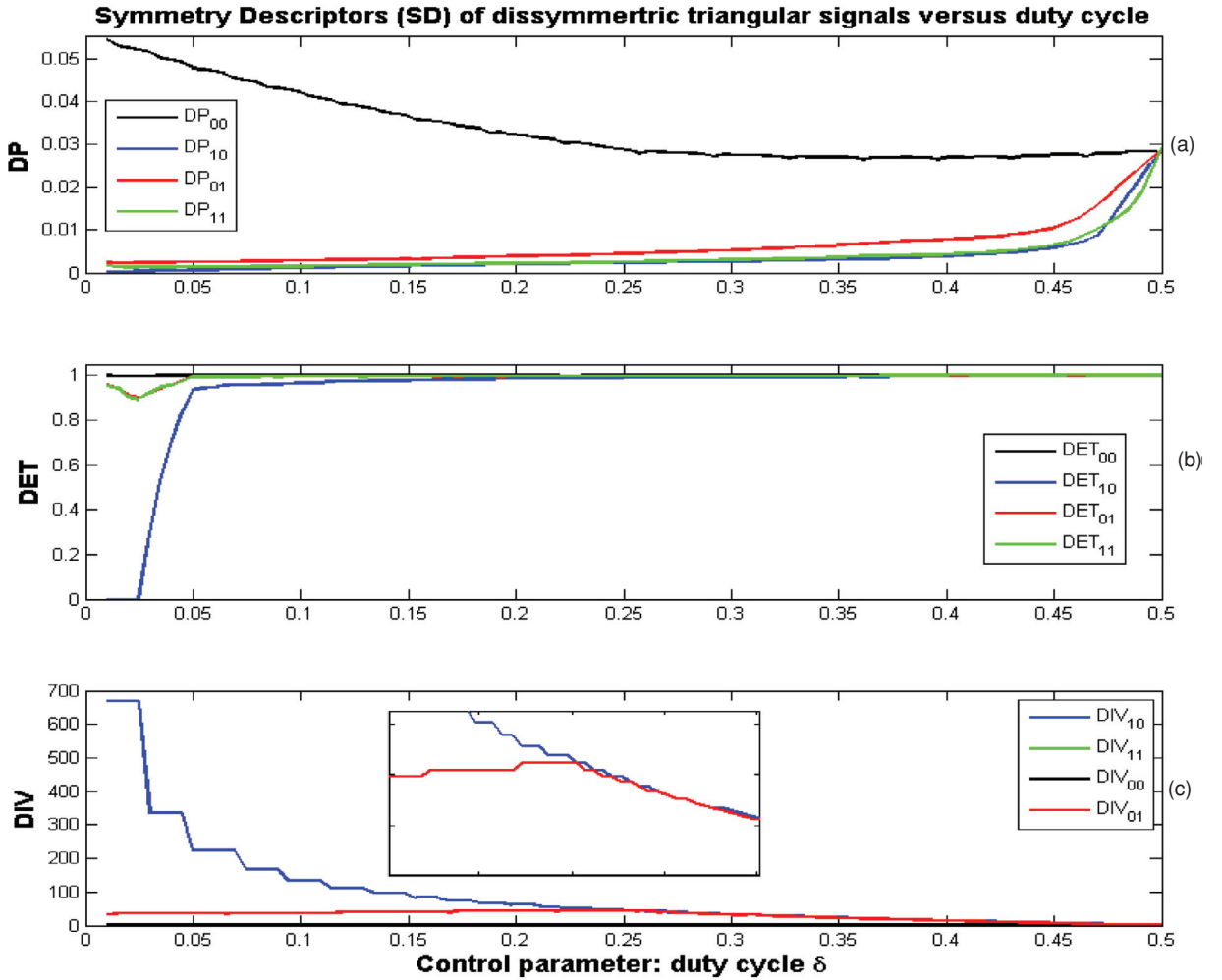


**Fig. 3.** SQA of dissymmetric triangular signals versus duty cycle  $\delta$ . (a)  $DP_{00}$ ,  $DP_{10}$ ,  $DP_{01}$  and  $DP_{11}$  versus the control parameter. Note that  $DIV_{01} \approx DIV_{11} \approx DIV_{10}$ . (b)  $DET_{00}$ ,  $DET_{10}$ ,  $DET_{01}$  and  $DET_{11}$  versus the control parameter. Note that  $DET_{00} \approx DET_{11} \approx DET_{01} \approx 1$ , confirming the deterministic nature of the time series. (c)  $DIV_{00}$ ,  $DIV_{10}$ ,  $DIV_{01}$  and  $DIV_{11}$  versus the control parameter. Note that  $DIV_{00} \approx 0$  and  $DIV_{11} = DIV_{01}$ , confirming the non-chaotic nature of the time series. Most of quantitative parameters were sensitive to variations in the control parameter (duty cycle).  $DET$  and  $DIV$  had opposite trends, when  $DET = 1$  then  $DIV = 0$  and when  $DET = 0$ , then  $DIV = 1$ . (For interpretation of the references to color in this figure legend, the reader is referred to the web version of this article.)

were calculated as follows:

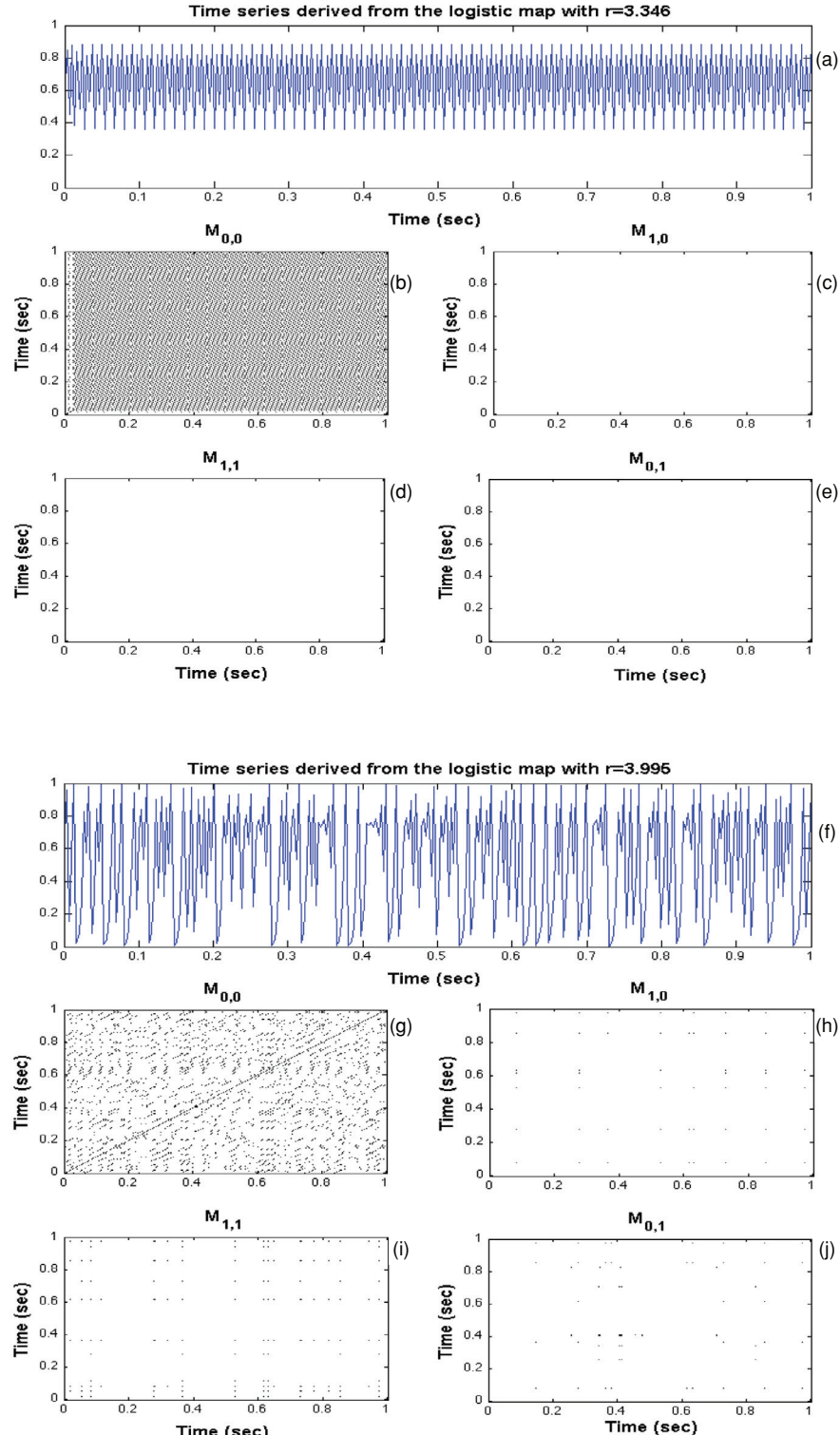
$$s_{i+1}(r) = rs_i(r)(1 - s_i(r)),$$

where  $s_0(r) = 0.5$ ,  $i$  varied in the range [1, 9] and  $r$  between 3.5 and 4. The intersection of  $s_i(r)$  with  $s_{i+j}(r)$  indicates the occurrence of a  $j$ -period cycle and the intersection of  $s_i(r)$  with the fixed-point  $(1 - 1/r)$  of the logistic map indicates the point of an unstable singularity, i.e. laminar behavior. Chaotic–chaotic transitions were obtained for  $s_i(r) = (1 - 1/r)$ .

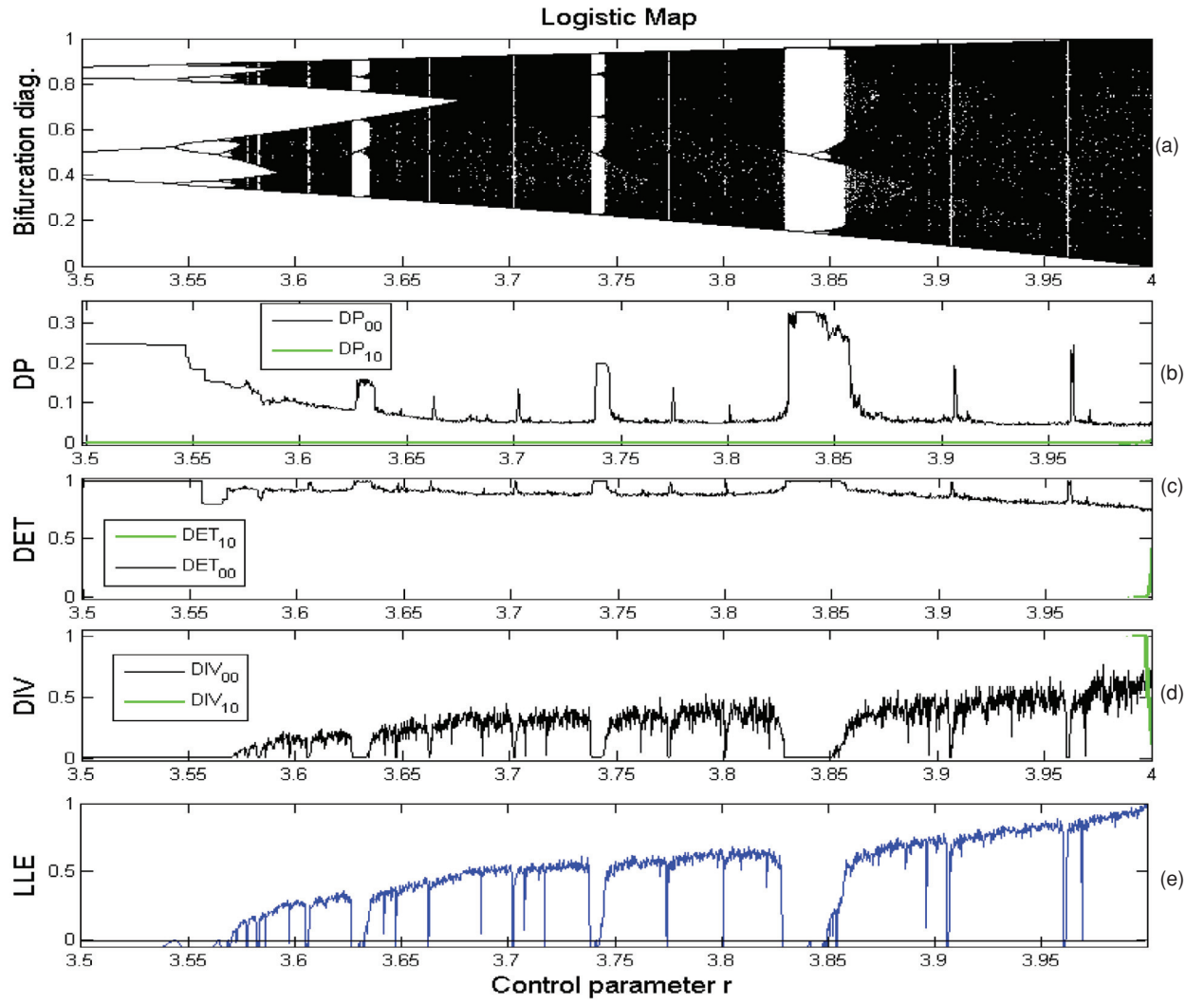
To be as representative as possible of different types of transition encountered in this kind of system, two time series derived from the logistic map obtained for  $r = 3.346$  and  $r = 3.995$  are shown as illustrations in Fig. 4a and f, respectively. Fig. 4b–e, g–j shows eight symmetry plots (SP) based on symmetry matrices  $M_{0,0}$ ,  $M_{1,0}$ ,  $M_{1,1}$ ,  $M_{0,1}$  obtained with  $\varepsilon = 10\%$  of the standard deviation of the time series. From

Fig. 4, it can be seen that certain SP contained many more symmetry points than others. However, it was not so much the number of symmetry points that was important but rather its variation in relation to the control parameters, as shown in Figs. 5 and 6.

Fig. 5a represents the bifurcation diagram of the logistic map when the control parameter  $r$  varied in the range [3.5, 4.0]. Fig. 5b–d represents symmetry descriptors (SD) of the first kind in relation to the control parameter. For  $p = q = 0$ , SD sensitive to the combination of translation invariances in  $x_1(n)$  and  $x_2(n)$  such as  $DP_{00}$ ,  $DET_{00}$  and  $DIV_{00}$  varied significantly (in the range [3.5, 4.0]). High sudden changes that occurred at periodic–periodic, periodic–chaotic and chaotic–periodic transitions can be easily observed in Fig. 5e whenever the LLE became just positive or negative, respectively. These outcomes were fairly similar to those obtained without embedding by Trulla et al. [5]. Note that for  $p = 1$  no significant variations were observed for  $DP_{10}$  since it was



**Fig. 4.** Symmetry plots (SP) of two time series derived from the logistic map. (a) Time series  $x_1$  with periodic behavior obtained for  $r = 3.546$ . (b) Matrix  $M_{0,0}$  of simple recurrences obtained from identity transformation with a non negligible number of identity recurrences. (c) Empty matrix  $M_{1,0}$  of opposite recurrences obtained from inversion transformation. (d) Empty matrix  $M_{1,1}$  of horizontal recurrences obtained from horizontal reflection. (e) Empty matrix  $M_{0,1}$  of vertical recurrences obtained from vertical reflection. (f) Time series  $x_1$  with chaotic behavior obtained for  $r = 3.995$ . Plots of opposite, horizontal and vertical recurrences are not fully empty, a small number of symmetry recurrences present. (g) Matrix of simple recurrences  $M_{0,0}$ . (h) Matrix  $M_{1,0}$  of opposite recurrences with small number of recurrences. (i) Matrix  $M_{1,1}$  of horizontal recurrences with few number of recurrences. (j) Matrix of vertical recurrences  $M_{0,1}$  with small number of recurrences.



**Fig. 5.** Symmetry descriptors (SD) of first kind derived from the logistic map for  $r$  ranging from 3.5 to 4 and for  $q = 0$ . Sudden changes appeared at periodic–periodic, periodic–chaotic and chaotic–periodic transitions. Symmetry descriptors obtained for  $p = 0$  and  $p = 1$  are depicted by black and green lines, respectively. (a) Bifurcation diagram. (b) Percentage of symmetric recurring points  $DP_{00}$  and  $DP_{10}$  versus the control parameter  $r$ .  $DP_{00}$  seemed to be sensitive to the periodic–chaotic bifurcations while  $DP_{10}$  seemed to be insensitive. (c) Percentage of symmetrical recurring points forming diagonals  $DET_{00}$  and  $DET_{10}$  versus  $r$ .  $DET_{00}$  seemed to be sensitive to the periodic nature of the time series while  $DET_{10}$  seemed to be insensitive. (d) Inverse of the longest diagonal  $DIV_{00}$  and  $DIV_{10}$  versus  $r$ .  $DIV_{00}$ , similar to LLE, seemed to be sensitive to the chaotic nature of the time series while  $DIV_{10}$  seemed to be insensitive. (e) Largest Lyapunov exponent (LLE) versus the control parameter. Chaotic regimes occur when LLE is positive. Note that because the matrix  $M_{10}$  was empty whatever the control parameter, the corresponding descriptors  $DP_{10}$  was null,  $DET_{10}$  and  $DIV_{10}$  were empty almost all the time. (For interpretation of the references to color in this figure legend, the reader is referred to the web version of this article.)

null everywhere, and  $DET_{10}$  and  $DIV_{10}$  were not defined due to the absence of diagonals. This means that the logistic map preferentially generated “simple” recurrences rather than opposite recurrences.

Fig. 6b–d represents symmetry descriptors (SD) of the second kind in relation to the control parameter. For  $q = 1$  and  $p = 0$ , SD sensitive to the combination of even symmetry in  $x_1(n)$  and odd symmetry in  $x_2(n)$  such as  $DP_{01}$ ,  $DET_{01}$  and  $DIV_{01}$  varied significantly (in the range [3.5, 4.0]). High sudden changes that occurred at chaotic–chaotic transitions can be easily observed in Fig. 6e whenever supertrack functions became equal to  $(1 - 1/r)$  (see dotted line in Fig. 6e). For  $q =$

1, SD possessed strong similarities to the “laminar” descriptors proposed by Marwan et al. [4]. This result was important since these descriptors had never been analyzed in relation to even (or vertical reflection) symmetry properties. No theoretical link exists between laminarity and even symmetry at this time. Demonstration of this relation will be the subject of another paper. Note that for  $p = 1$  and  $q = 1$ , no significant variations were observed for  $DP_{11}$ ,  $DET_{11}$  and  $DIV_{11}$ . This means that the logistic map generated even rather than odd symmetry. This was also very surprising since the logistic map is normally unable to generate even symmetries. This point can be understood and accepted if it is assumed

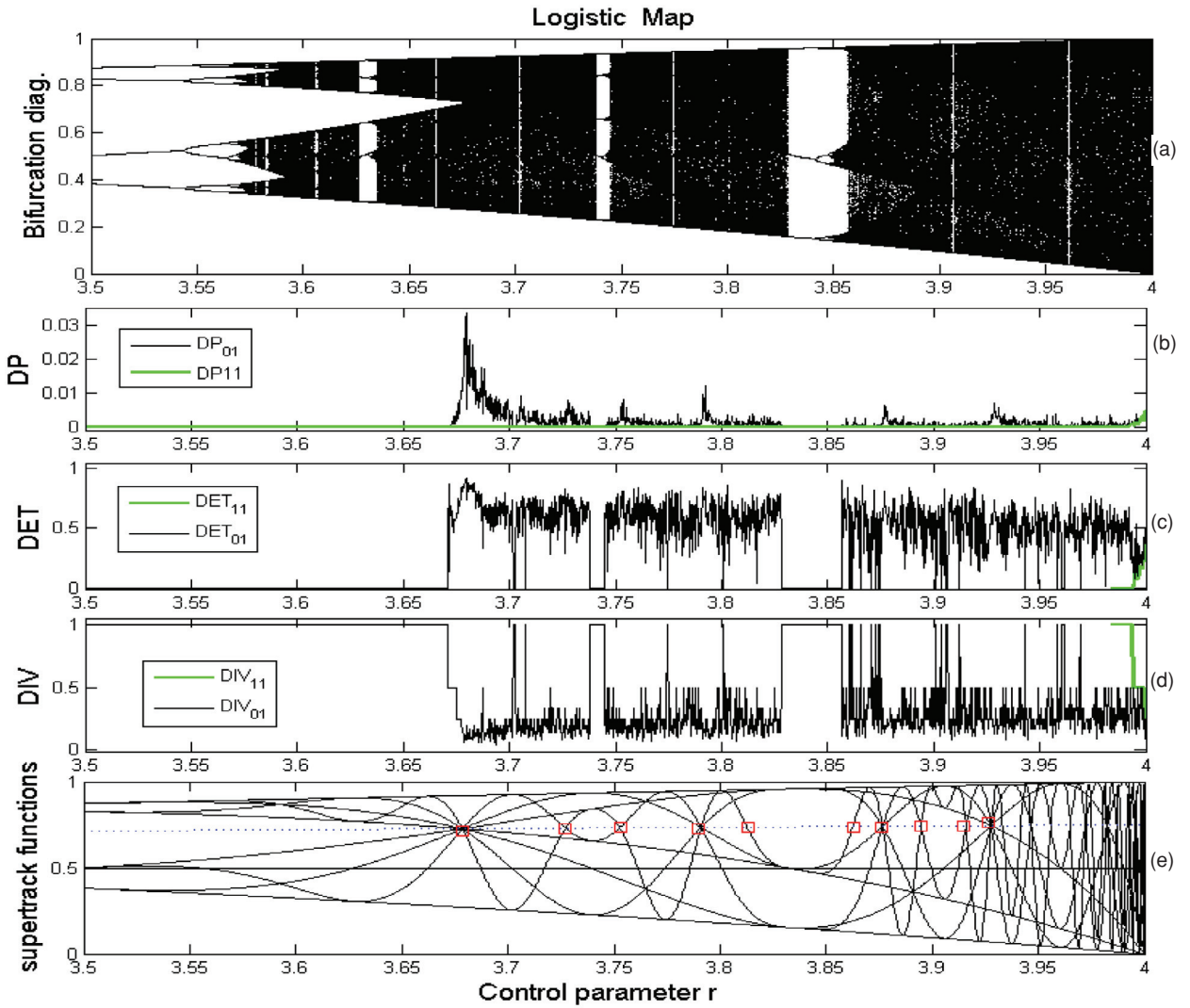


**Fig. 6.** Symmetry descriptors (SD) of second kind derived from the logistic map for  $r$  ranging from 3.5 to 4 and for  $q = 1$ . Sudden changes appeared at periodic-periodic, periodic-chaotic and chaotic-periodic transitions. Symmetry descriptors obtained for  $p = 0$  and  $p = 1$  are depicted by black and green lines, respectively. (a) Bifurcation diagram. (b) Percentage of symmetrical recurrence points  $DP_{01}$  and  $DP_{11}$  versus the control parameter  $r$ .  $DP_{01}$  seemed to be sensitive to chaotic-chaotic bifurcations while  $DP_{11}$  seemed to be insensitive. (c) Percentage of symmetrical recurrence points forming diagonals  $DET_{01}$  and  $DET_{11}$  versus  $r$ .  $DET_{01}$  seemed to be sensitive to the chaotic-chaotic bifurcations while  $DET_{11}$  seemed to be insensitive. (d) Inverse of the longest diagonal  $DIV_{01}$  and  $DIV_{11}$  versus  $r$ . Similar to LLE,  $DIV_{01}$  seemed to be sensitive to the chaotic-chaotic bifurcations while  $DIV_{11}$  seemed to be insensitive. (e) Supertrack functions  $s_i(r)$  versus control parameter  $r$ . A few chaotic-chaotic transitions (represented by red squares) occurred when  $s_i(r) = 1 - 1/r$  (dotted line). Note that because the matrix  $M_{10}$  was empty whatever the control parameter, the corresponding descriptors  $DP_{11}$  was null,  $DET_{11}$  and  $DIV_{10}$  were empty almost all the time. (For interpretation of the references to color in this figure legend, the reader is referred to the web version of this article.)

that the even symmetries generated were local and not global.

To summarize this section, the logistic map showed a certain insensitivity to symmetries obtained with  $p = 1$  (odd symmetry and opposite recurrence), while it demonstrated marked sensitivity to symmetry obtained with  $p = 0$  (even symmetry and simple recurrence). Finally, a more complete view of the logistic map can be proposed due to the general framework of symmetry.

In order to demonstrate that the symmetry framework is still capable of describing symmetry obtained when  $p = 1$ , the cubic map is examined in the next section.

#### 4.2. The cubic map

The cubic map described by [26–28] was investigated as a second example:

$$x_{n+1} = r(x_n - x_n^3), \quad (22)$$

where the control parameter  $r$  varies in the range  $[0.5, 3.0]$ . This system, that possesses global odd symmetry, is invariant under a symmetrical operation:  $x \rightarrow -x$ . This discrete system possesses the particular feature of having three types of operating regime [27,28]:

- when  $r < 1$ , the stable point  $x = 0$  satisfies the symmetry;

- when  $r > 1$ , the system loses its symmetry. The critical point  $r_c = 1$  is a bifurcation point of “symmetry-breaking”;
- the system recovers its symmetry for  $r > \frac{3\sqrt{3}}{2}$ . The critical point  $r_s = \frac{3\sqrt{3}}{2}$  is a bifurcation point of “symmetry-increasing”.

As the main goal was to detect different kinds of bifurcation point such as “symmetry increasing” and “symmetry breaking”, the largest Lyapunov exponent  $\lambda$  and supertrack functions were evaluated:

- The largest Lyapunov exponent (LLE) defined as follows:

$$\lambda = \frac{1}{N} \sum_{n=1}^N \log_2 |r(1 - 3x_n^2)|$$

was evaluated in relation to the control parameter  $r$ , as suggested by [27,28]. Note that the chaotic regimes were present when the largest Lyapunov exponent was positive  $\lambda > 0$ .

- As for the standard logistic map, to observe the presence of chaotic-chaotic transitions, recursive functions named “supertrack” were calculated as follows:

$$s_{i+1}(r) = rs_i(r)(1 - s_i^2(r)),$$

where  $s_0(r) = 0.5$ ,  $i$  varied in the range [1, 7] and  $r$  in the range [2.2, 3]. The intersection of  $s_i(r)$  with  $s_{i+j}(r)$  indicates the occurrence of a  $j$ -period cycle, and the intersection of  $s_i(r)$  with the fixed-point  $\sqrt{1 - 1/r}$  of the cubic map indicates the point of unstable singularity, i.e. laminar behavior. Chaotic-chaotic transitions were obtained for  $s_i(r) = \sqrt{1 - 1/r}$ .

To be as representative as possible of different types of transition encountered in this kind of system, two time series derived from the cubic map obtained for  $r = 2.394$  and  $r = 2.604$  are shown as illustrations in Fig. 7a and f, respectively.

Fig. 7b–e, g–j shows eight symmetry plots (SP) based on the symmetry matrices  $M_{0,0}$ ,  $M_{0,1}$ ,  $M_{1,0}$ ,  $M_{1,1}$  and obtained with  $\varepsilon = 10\%$  of the standard deviation of the time series. It can be seen from Fig. 7, that  $M_{0,0}$  contained a large number of recurrence points compared to the other matrices that possessed few symmetry points. Moreover, the number of symmetry points was higher with  $r = 2.604$  than with  $r = 2.394$ . This was particularly true for  $M_{1,0}$  (see Fig. 7c). However, it was not so much the number of symmetry points that was important but rather their variation in relation to the control parameters, as shown in Figs. 8–10.

Fig. 8a represents the bifurcation diagram of the cubic map when the control parameter varied in the range [0.5, 3.0]. Fig. 8b–g represents symmetry descriptors (SD) in relation to the control parameter. From Fig. 8, it is easy to identify the bifurcation point of “symmetry-breaking” occurring at  $r_c = 1$  and the bifurcation point of “symmetry-increasing” occurring at  $r_s = 3\sqrt{3}/2 \approx 2.60$ . Note also that bifurcation points of a doubling-period can be easily identified, as is the case for  $r = 2$  (see arrow in Fig. 8b). Areas where the cubic map lost and recovered its symmetry are indicated by red double arrows.

Fig. 9a represents the bifurcation diagram of the cubic map when the control parameter  $r$  varied in the range [2.2, 3.0]. Fig. 9b–d represents symmetry descriptors (SD) of the first kind in relation to the control parameter. SD sensitive

to simple recurrence such as  $DP_{00}$ ,  $DET_{00}$  and  $DIV_{00}$  varied significantly (in the range [2.2, 3.0]). High sudden changes that occurred at periodic-chaotic and chaotic-periodic transitions can be easily observed in Fig. 9e whenever the LLE became just positive or negative, respectively. Note that significant variations were observed for  $DP_{10}$ ,  $DET_{10}$  and  $DIV_{10}$  when the control parameter was greater than  $r_s \approx 2.60$ . In the range [2.6, 3.0],  $DP_{00}$ ,  $DET_{00}$  and  $DIV_{00}$  were similar to  $DP_{10}$ ,  $DET_{10}$  and  $DIV_{10}$ , respectively (curves superimposed). This means that the cubic map generated both simple recurrences and opposite recurrences. Note that  $DP_{10}$ ,  $DET_{10}$ ,  $DIV_{10}$  were always superimposed on  $DP_{00}$ ,  $DET_{00}$ ,  $DIV_{00}$  except for one peak indicated by a red arrow at  $r = 2.868$ . This strange behavior has not been explained to date and needs further study.

Fig. 10b–d represents symmetry descriptors (SD) of the second kind in relation to the control parameter. SD sensitive to even symmetry such as  $DP_{01}$ ,  $DET_{01}$  and  $DIV_{01}$  varied significantly (in the range [2.2, 3.0]). High sudden changes that occurred at chaotic-chaotic transitions can be easily observed in Fig. 10e whenever supertrack functions became equal to  $\sqrt{1 - 1/r}$ . These SD possessed strong similarities to the “laminar” descriptors proposed by Marwan et al. [4]. Note that significant variations were observed for  $DP_{11}$ ,  $DET_{11}$  and  $DIV_{11}$  when the control parameter was greater than  $r_s \approx 2.60$ . In the range [2.6, 3.0],  $DP_{01}$ ,  $DET_{01}$  and  $DIV_{01}$  were similar to  $DP_{11}$ ,  $DET_{11}$  and  $DIV_{11}$ , respectively (curves superimposed). Note that  $DP_{11}$ ,  $DET_{11}$ ,  $DIV_{11}$  were always superimposed on  $DP_{01}$ ,  $DET_{01}$ ,  $DIV_{01}$  except for a few peaks indicated by red arrows. This strange behavior has been not explained to date and needs further study. Nevertheless, this means that the cubic map generated both even and odd symmetries almost all the time, which was very surprising since the cubic map is normally unable to generate even symmetries. This can be understood and accepted if it is assumed that the even symmetries generated were local and not global.

To sum up this section, symmetrical descriptors were found to be sensitive to operating regime changes involving “broken-symmetry”, “increased-symmetry”, “periodic-periodic”, “periodic-chaotic”, “chaotic-periodic” and “chaos-chaos” transitions. Testing several symmetrical descriptors was important since they each had different sensitivity despite being subjected to the same operating change. This supports the idea that such symmetric descriptors are undeniable for the precise characterization of nonlinear dynamical systems.

## 5. Discussion and conclusion

Symmetries present in a geometrical object can currently be studied using a certain number of theoretical tools [30]. However, no simple numerical tools have been available to date to allow study of intrinsic symmetries of time series, as is the case with recurrence.

Such numerical tools were proposed in this study, in particular by introducing the isometry concept and then adapting its formulation for time series, thus proposing a general framework including the recurrence concept. New kinds of recurrence (translation/reversal) were proposed and four symmetries were studied: the symmetry matrix of identity corresponding to simple recurrences (translations in the time

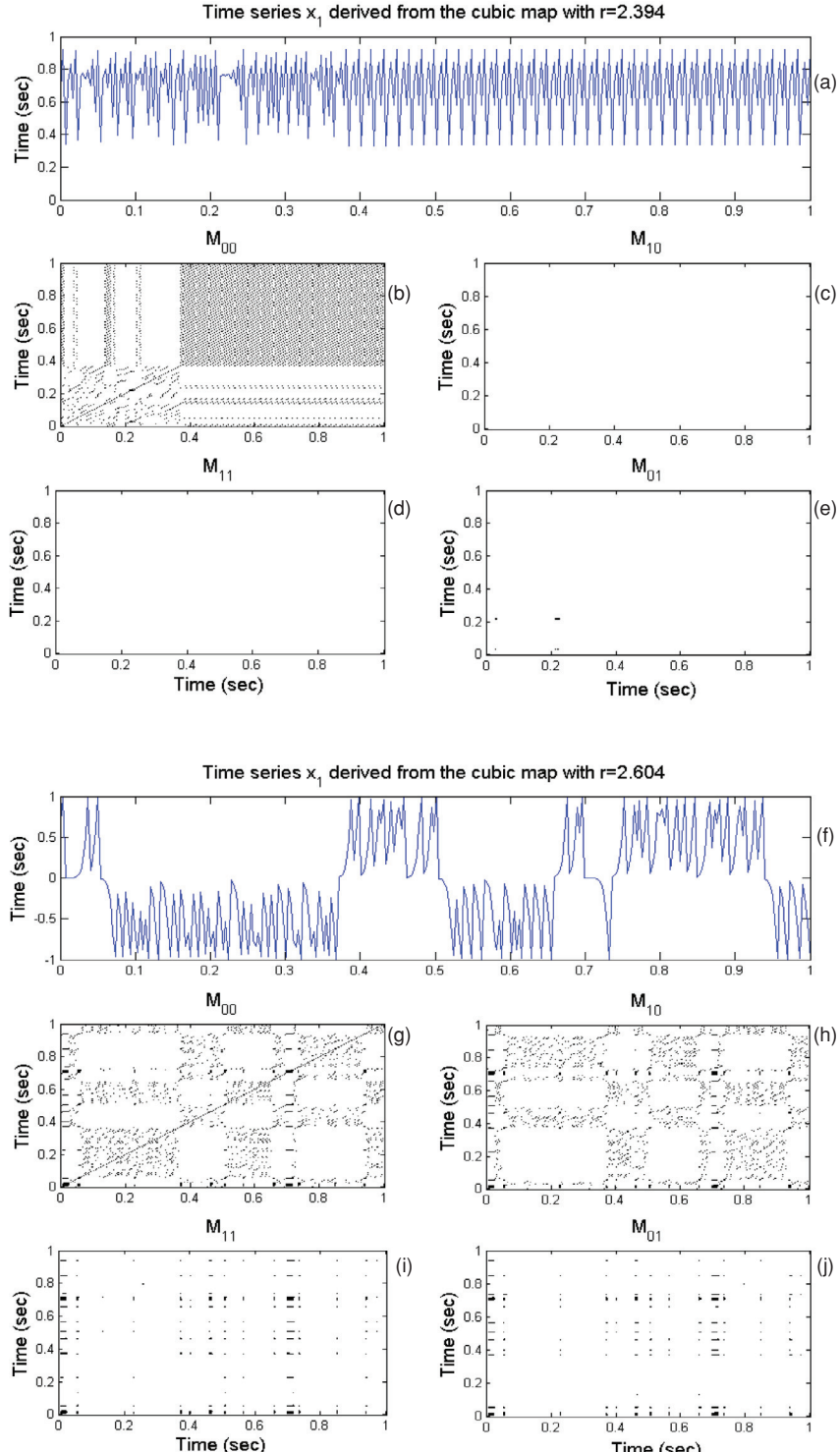


**Fig. 7.** Symmetry plots (SP) of two time series derived from the cubic map. (a) Time series  $x_1$  with chaotic behavior obtained for  $r = 2.394$ . In that range the system lost its odd symmetry. Except for the recurrences, a low level of symmetry seemed to be present in this time series. Plots of opposite and odd recurrences were empty. (b) Matrix  $M_{00}$  of recurrences obtained from identity transformation. (c) Empty matrix  $M_{10}$  of opposite recurrences obtained from inversion transformation. (d) Empty matrix  $M_{11}$  of horizontal recurrences obtained from horizontal reflection. (e) Matrix  $M_{01}$  of vertical recurrences obtained from vertical reflection with small number of even recurrences. (f) Time series  $x_1$  with chaotic behavior obtained for  $r = 3.995$ . In this range the system recovered its odd symmetry. Plots of opposite, horizontal and vertical recurrences were not fully empty, a small number of symmetry recurrences was present. (g) Matrix  $M_{00}$  of simple recurrences with a non-negligible number of identity recurrences. (h) Matrix  $M_{10}$  of opposite recurrences with a non-negligible number of opposite recurrences. (i) Matrix  $M_{11}$  of horizontal recurrences with small number of recurrences. (j) Matrix  $M_{01}$  of vertical recurrences with small number of recurrences.

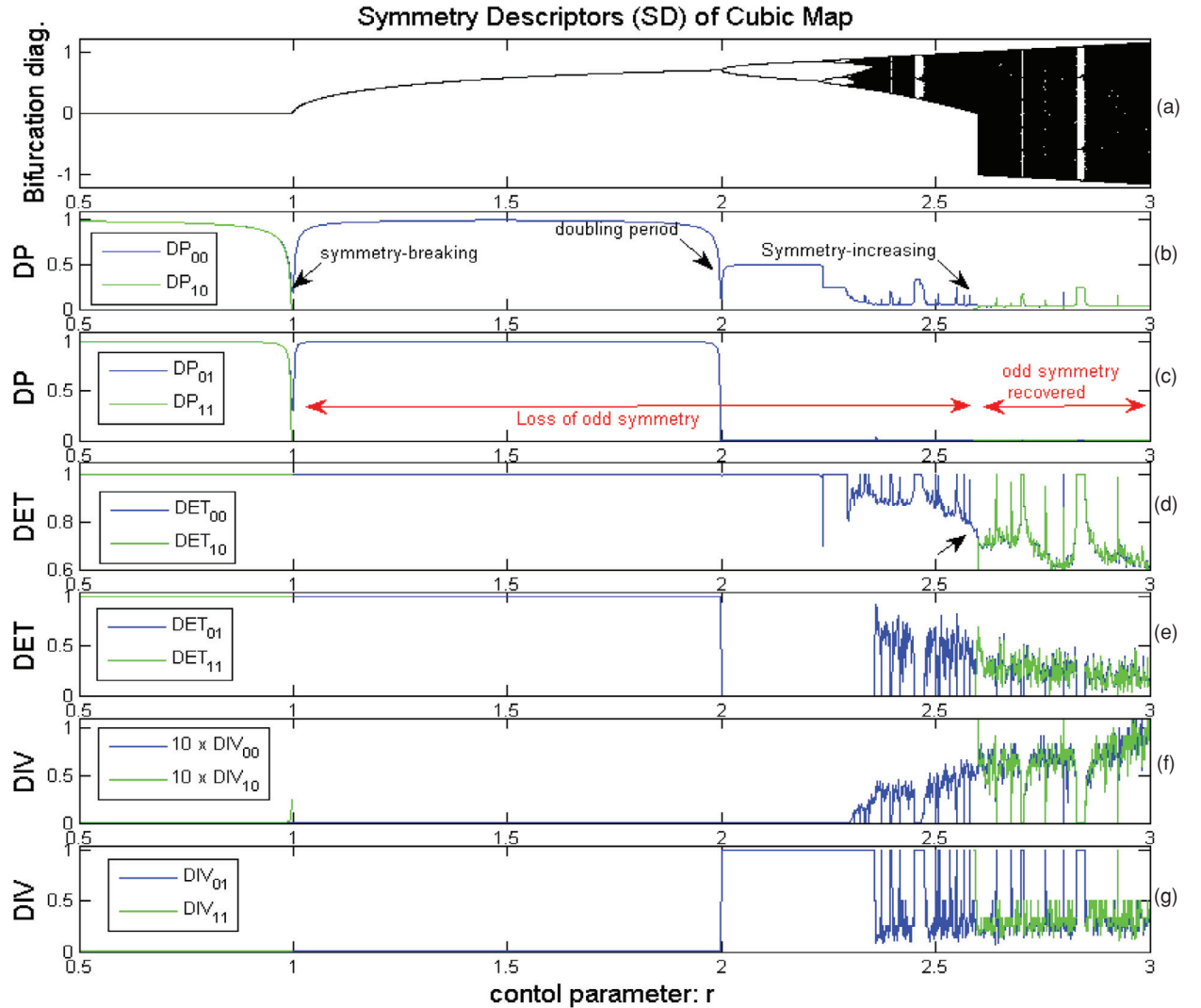


**Fig. 8.** Symmetry descriptors (SD) derived from the cubic map for  $r$  ranging from 0.5 to 3.0. (a) Bifurcation diagram. (b)  $DP_{00}$  green line and  $DP_{10}$  blue line. (c)  $DP_{01}$  green line and  $DP_{11}$  blue line. (d)  $DET_{00}$  green line and  $DET_{10}$  blue line. (e)  $DET_{01}$  green line and  $DET_{11}$  blue line. (f)  $DIV_{00}$  green line and  $DIV_{10}$  blue line. (g)  $DIV_{01}$  green line and  $DIV_{11}$  blue line. Sudden changes were related to transitions. The two critical bifurcation points of "broken-symmetry" ( $r_c = 1$ ), and "increased-symmetry" ( $r_s = 3\sqrt{3}/2 \approx 2.6$ ) were clearly located (see black arrows). Before the period-doubling transition  $DET_{pq} \approx 1$  and  $DIV_{pq} \approx 0$ , suggesting deterministic nature of the time series whatever the kind of symmetry. (For interpretation of the references to color in this figure legend, the reader is referred to the web version of this article.)

series), the symmetry matrix of vertical reflections corresponding to vertical recurrences (even/odd symmetries in the time series), the symmetry matrix of inversions corresponding to opposite recurrences (glide symmetry in the time series) and finally the symmetry matrix of horizontal reflections corresponding to horizontal recurrences (odd symmetry and translation in the time series). These matrices resulted in a binary test composed of two conditions, each relating to a norm. Note that, although the Euclidean norm was chosen here, other types of norm may be used such as the maximum norm or the Manhattan norm.

From this study, in which symmetry quantification analysis (SQA) was applied, it was shown that most transitions

and bifurcation points were detected with only three symmetry descriptors. Indeed, from the discrete periodic time series and discrete chaotic time series derived from the logistic and cubic maps that were analyzed, it was demonstrated that the symmetry descriptors proposed were very sensitive and effective in detecting a wide variety of regime changes commonly encountered in nonlinear dynamical systems.

On the other hand, it was shown that it was possible to establish the presence of global symmetry and unexpected local symmetries. This means that, even when a nonlinear dynamical system possesses a certain kind of global symmetry, such a system can generate *a priori* unexpected local

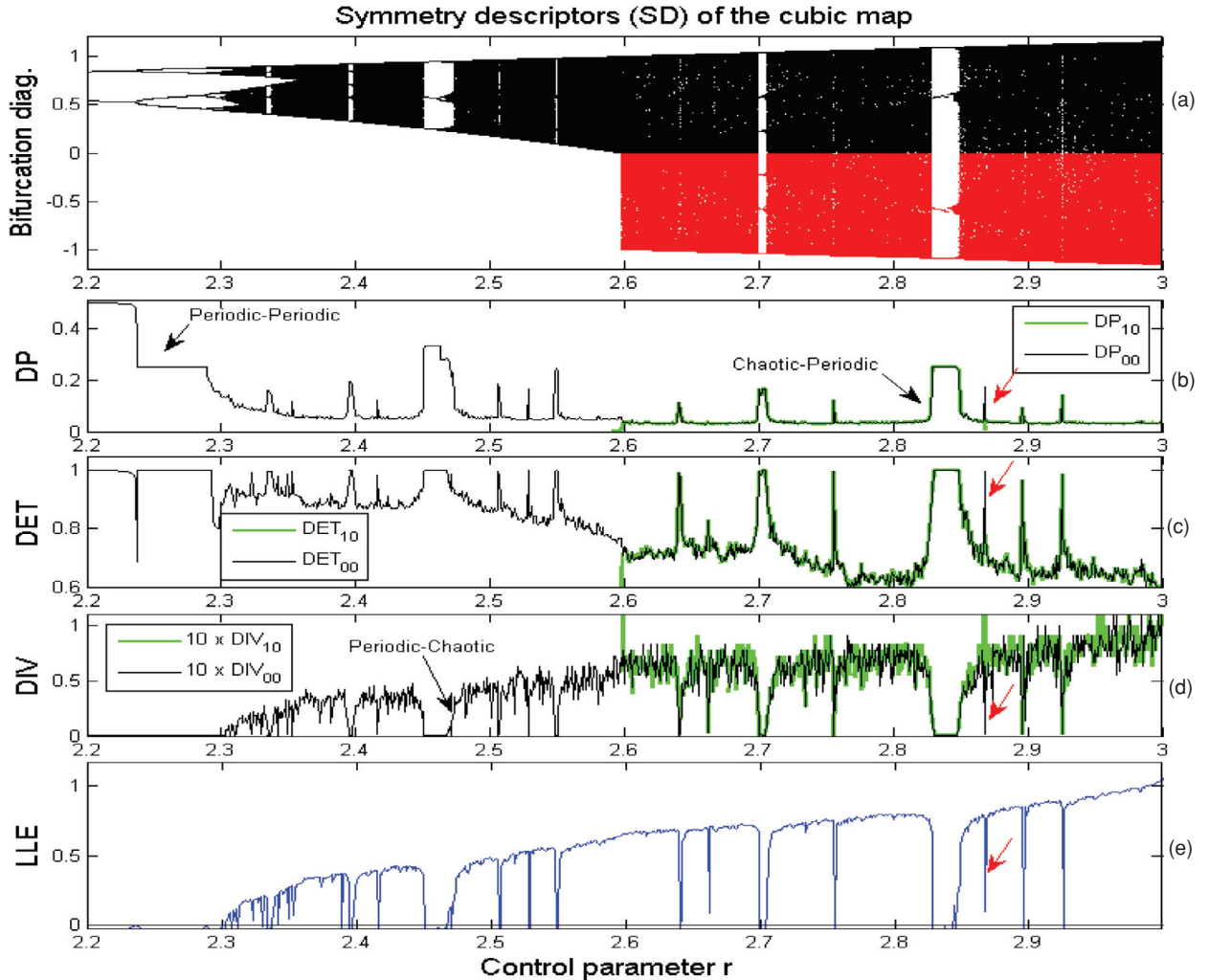


**Fig. 9.** Symmetry descriptors (SD) of the first kind derived from the cubic map for  $r$  ranging from 2.2 to 3 and for  $q = 0$ . Sudden changes present in SD were related to transitions. The red area ranging from 2.6 to 3 corresponded to the recovering symmetry area. (a) Bifurcation diagram. (b)  $DP_{00}$  black line and  $DP_{10}$  green line. (c)  $DET_{00}$  black line and  $DET_{10}$  green line. (d)  $DIV_{00}$  black line and  $DIV_{10}$  green line. (e) Largest Lyapunov exponent (LLE) versus control parameter. Chaotic regimes occurred when LLE was positive i.e. outside the green area. The few periodic-periodic, periodic-chaotic and chaotic-periodic transitions are identified by black arrows. The antinomic nature of  $DET$  and  $DIV$  is verified since  $DET \approx 1$  and  $DET \approx 0$ . At the right of  $r_s \approx 2.6$ , SP with  $p = 1$  are insignificant since the symmetry was lost. At the left of  $r_s \approx 2.6$ , all SP are significant since the symmetry was recovered. Green curves (with  $p = 1$ ) are always superimposed except for one peak indicated by a red arrow at  $r = 2.868$ . (For interpretation of the references to color in this figure legend, the reader is referred to the web version of this article.)

symmetries that can contribute to the characterization and the understanding of the system in a non-negligible way.

However, it appears that both the identification of global and local symmetries and the precise detection of chaotic-periodic, periodic-chaotic [5], chaotic-chaotic transitions [4], “symmetry-breaking” bifurcations [28,29,31,33] and “symmetry-increasing” bifurcations [27] constitute promising results that bode well for the future, particularly in fields such as meteorology, finance and biomedicine. Indeed, the assessment of symmetry descriptors could be advantageously introduced for direct detection of symmetry breaking phenomena from the phase space (or time series) when the symmetry parameter varies.

It is also of note that, though not tested in this study, the proposed numerical tools still work on continuous dynamical systems as such the Helmholtz-Duffing system analyzed in greater depth in [7]. Consequently, all studies using recurrence plots can be redone with symmetry plots, as simple recurrences are a particular case of new recurrences with symmetry.

To conclude, although certain issues remain to be resolved, this new framework marks considerable progress in the study of time series derived from dynamical systems of low dimensions since it allows the numerical detection of transitions from a hitherto unknown kind of symmetry descriptor.

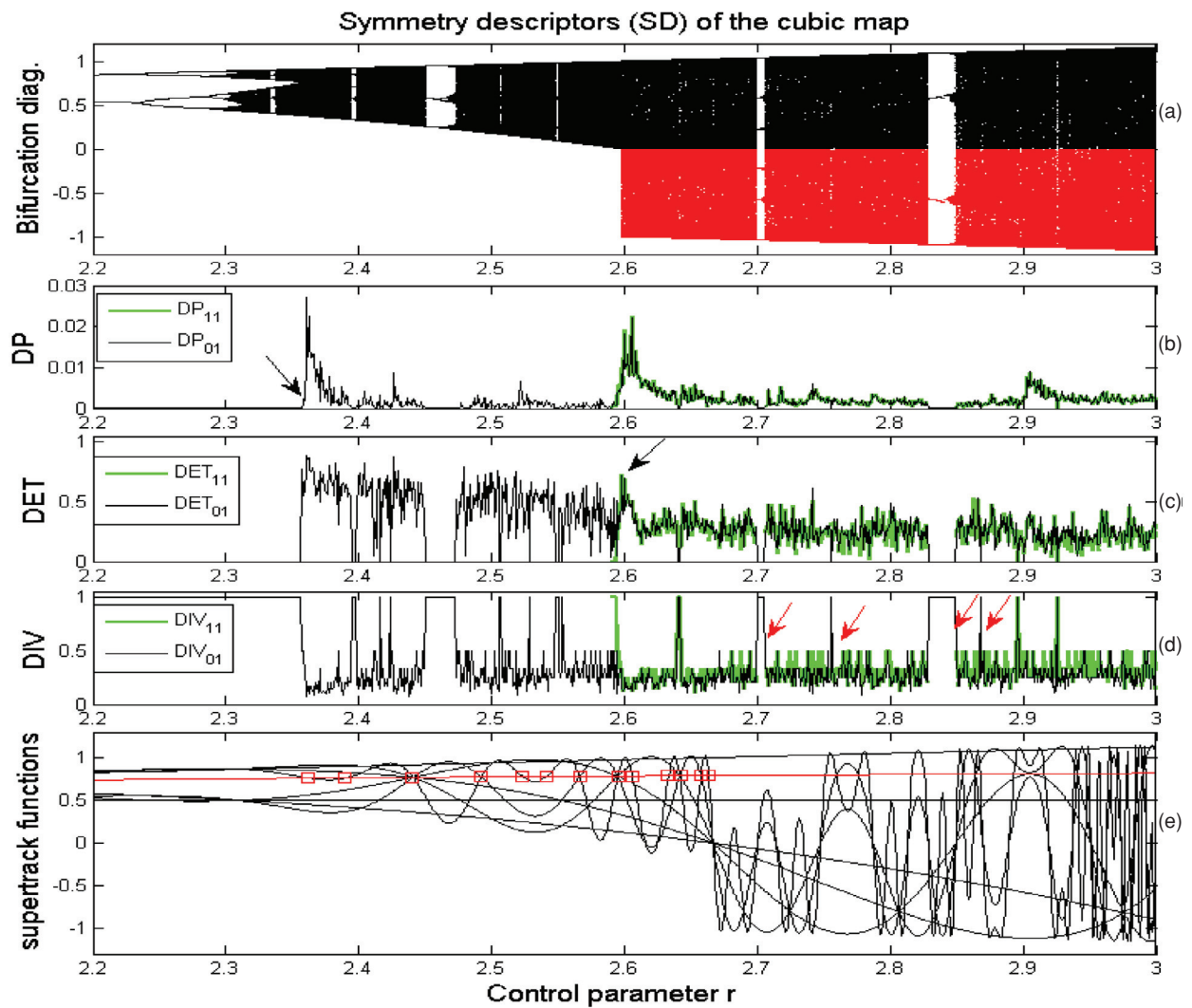


**Fig. 10.** Symmetry descriptors (SD) of second kind derived from the cubic map for  $r$  ranging from 2.2 to 3 and for  $q = 1$ . Sudden changes present in SD were related to transitions. The red area ranging from 2.6 to 3 corresponded to the recovering symmetry area. (a) Bifurcation diagram. (b)  $DP_{01}$  black line and  $DP_{11}$  green line. (c)  $DET_{01}$  black line and  $DET_{11}$  green line. (d)  $DIV_{01}$  black line and  $DIV_{11}$  green line. (e) Supertrack functions  $s_i(r)$  versus control parameter. A few chaotic-chaotic transitions (red squares) occurred when  $s_i(r) = \sqrt{1 - 1/r}$  (red line). The antinomic nature of  $DET$  and  $DIV$  is verified since  $DET \approx 1$  and  $DET \approx 0$ . At the right of  $r_s \approx 2.6$ , SP with  $p = 1$  are insignificant since symmetry was lost. At the left of  $r_s \approx 2.6$ , all SP are significant since symmetry was recovered. Green curves (with  $p = 1$ ) are always superimposed except for a few peaks indicated by red arrows. (For interpretation of the references to color in this figure legend, the reader is referred to the web version of this article.)

## References

- [1] Millan H, Kalauzi A, Llerena G, Sucoshanay J, Piedra D. Meteorological complexity in the Amazonian area of Ecuador: an approach based on dynamical system theory. *Ecol Complex* 2009;6:278.
- [2] Marwan N, Trauth MH, Vuille M, Kurths J. Comparing modern and Pleistocene ENSO-like influences in NW Argentina using nonlinear time series analysis methods. *Climate Dyn* 2003;21:317.
- [3] Mestivier D, Chau NP, Chanudet X, Bauduceau B, Larroque P. Relationship between diabetic autonomic dysfunction and heart rate variability assessed by recurrence plot. *Am J Physiol – Heart Circ Physiol* 1997;272:1094.
- [4] Marwan N, Wessel N, Meyerfeldt U, Schirdewan A, Kurths J. Recurrence-plot-based measures of complexity and their application to heart-rate-variability analysis. *Phys Rev E* 2002;66:026702.
- [5] Trulla L, Giuliani R, Zbilut J, Webber C. Recurrence quantification analysis of the logistic equation with transients. *Phys Lett A* 1996;223:255.
- [6] Souza EG, Viana RL, Lopes SR. Using recurrences to characterize the hyperchaos–chaos transition. *Phys Rev E* 2008;78:066206.
- [7] Cao H, Seoane JM, Sanjuan MA. Symmetry breaking analysis for the general Helmholtz–Duffing oscillator. *Chaos Solitons Fractals* 2007;34:197.
- [8] Eckmann J-P, Kamphorst S, Ruelle D. Recurrence plots of dynamical systems. *Europhys Lett* 1987;4:973.
- [9] Marwan N. Encounters with neighbours-current developments of concepts based on recurrence plots and their applications Phd thesis. Postdam: Institute of Physics, University of Postdam; 2003.
- [10] Marwan N, Romano MC, Thiel M, Kurths J. Recurrence plots for the analysis of complex systems. *Phys Rep* 2007;438:237.
- [11] Iwanski JS, Bradley E. Recurrence plot analysis: to embed or not to embed? *Chaos* 1998;8:861.
- [12] Babinec P, Zemavova L, Babincova M. Randomness and determinism in human heart-beat dynamics: recurrence plot analysis. *Phys Med* 2002;18:63.
- [13] Rosso OA, Larrondo HA, Martin MT, Plastino A, Fuentes MA. Distinguishing noise from chaos. *Phys Rev Lett* 2007;99:154102.
- [14] Webber CL, Marwan N, Faccini A, Giuliani A. Simpler methods do it better: success of recurrence quantification analysis as a general purpose data analysis tool. *Phys Lett A* 2009;373:3745.

- [15] Webber CL, Zbilut JP. Dynamical assessment of physiological systems and states using recurrence plot strategies. *J Appl Physiol* 1994;76:965.
- [16] Zbilut JP, Webber CL, Colosimo A, Giuliani A. The role of hydrophobicity patterns in prion folding as revealed by recurrence quantification analysis of primary structure. *Protein Eng* 2000;13:99.
- [17] Zbilut JP, Thomasson N, Webber CL. Recurrence quantification analysis as a tool for nonlinear exploration of nonstationary cardiac signals. *Med Eng Phys* 2002;24:53.
- [18] Fabretti A, Ausloos M. Recurrence plot and recurrence quantification analysis techniques for detecting a critical regime. Examples from financial market indices. *Int J Mod Phys C* 2005;16:671.
- [19] Karakasidis TE, Fragkou A, Liakopoulos A. System dynamics revealed by recurrence quantification analysis: application to molecular dynamics simulations. *Phys Rev E* 2007;76:021120.
- [20] Zbilut JP, Webber CL. Embeddings and delays as derived from quantification of recurrence plots. *Phys Lett A* 1992;171:199.
- [21] Weyl H. Symmetry. Princeton, Princeton University Press; 1952.
- [22] Field M, Golubitsky M. Symmetry in chaos: a search for pattern in mathematics, art and nature. Oxford: Oxford University Press; 1992.
- [23] Allgower EL, Georg K, Miranda R. Exploiting symmetry in applied and numerical analysis. American Mathematical Society; 1995.
- [24] Cantwell BJ, Crighton DG. Introduction to symmetry analysis. Cambridge University Press; 2002.
- [25] Gilmore R, Letellier C. The symmetry of chaos. Oxford University Press; 2007.
- [26] May R. Mathematical modelling: the cubic map in theory and practice. *Nature* 1984;311:13–144.
- [27] Chossat P, Golubitsky M. Symmetry-increasing bifurcation of chaotic attractors. *Phys D* 1988;32:423.
- [28] Lai YC. Symmetry-breaking bifurcation with on-off intermittency in chaotic dynamical systems. *Phys Rev E* 1996;53:R4267.
- [29] Isohätälä J, Alekseev KN, Kurki LT, Pietiläinen P. Symmetry breaking in a driven and strongly damped pendulum. *Phys Rev E* 2005;71:066201–6.
- [30] Barany E, Dellnitz M, Golubitsky M. Detecting the symmetry of attractors. *Phys D* 1993;67:66.
- [31] Tchistiaikov V. Detecting symmetry breaking bifurcation in the system describing the dynamics of coupled arrays of Josephson junctions. *Phys D* 1996;91:67.
- [32] Letellier C, Aguirre LA. Investigating nonlinear dynamics from time series: the influence of symmetries and the choice of observables. *Chaos* 2002;12:549.
- [33] Lai YC. Scaling laws for symmetry breaking by blowout bifurcation in chaotic systems. *Phys Rev E* 1997;56:1407.
- [34] Thiel M, Romano MC, Read P, Kurths J. Estimation of dynamical invariants without embedding by recurrence plots. *Chaos* 2004;14:234.
- [35] March TK, Chapman SC, Dendy RO. Recurrence plot statistics and the effect of embedding. *Phys D* 2005;200:171.
- [36] Zaylaa A, Charara J, Girault J-M. Reducing sojourn points from recurrence plots to improve transition detection: application to fetal heart rate transitions. 2014. CBM, 2014, Oct 2. pii: S0010-4825(14)00258-3. doi:<http://dx.doi.org/10.1016/j>
- [37] Grassberger P, Procaccia I. Measuring the strangeness of strange attractors. *Phys D* 1983;9:189.
- [38] Krese B, Perc M, Govekar E. Experimental observation of chaos-chaos transition in LASER droplet generation. *Int J Bifur Chaos* 2011;21:1689.
- [39] Dodge CW. Euclidean geometry and transformations. Mineola, New York: Dover Publications Inc.; 1972.